Dissertation for the Degree of Doctor of Philosophy

Development of Graphene-Reinforced Bone Cements and Characteristics of Graphene-Based Platform with Electromagnetic Field

February, 2016

by

Hoon Seonwoo

Department of Biosystems & Biomaterials Science and Engineering

Major in Biosytems Engineering

Seoul National University

Development of Graphene-Reinforced Bone Cements and Characteristics of Graphene-Based Platform with Electromagnetic Field

by

Hoon Seonwoo

Submitted to the Department of Biosystems & Biomaterials Science and Engieering
in Partial Fulfillment of the Requirements for the Degree of

Doctor of Philosophy in Biosystems Engineering

at the

Seoul National University

February 2016

Jong Hoon Chung, Ph.D._____
Dissertation Advisor
Professor of Departement of Biosystems & Biomaterials Science and Engineering
Seoul National University

Ghiseok Kim, Ph.D._____
Professor of Departement of Biosystems & Biomaterials Science and Engineering
Seoul National University

Ki Taek Lim, Ph.D._____
Professor of Department of Biosystems Engineering
Kangwon National University

Yun-Hoon Choung, M.D., D.D.S., Ph.D._____
Professor of Department of Otolaryngology
Ajou University School of Medicine

GeunHyung Kim, Ph.D._____
Professor of Department of Bio-Mechatronic Engineering
Sungkyunkwan University

Abstract

Tissue engineering is the study to reconstruct tissue and organs of living things by applying material science engineering and biological principles. It has been reported that according to the change of size, shape, and conformation of nanostructure, cellular adhesion, proliferation, and differentiation can be modulated. In other words, regulation of nanostructure can engineer cellular fate. Another method to control cellular function is using nanomaterials. The nanomaterials can derive synergic effects if the nanomaterials have additional functionality. Nowadays, graphene is getting spotlight. The graphene, recently discovered in 2004, also have high thermal and electrical conductivity, large specific surface area, and good mechanical properties. Further, it can be functionalized, indicating graphene can be used as diverse forms. Due to those unique characteristics, the graphene have been frequently used in biosensors, drug delivery, and gene delivery but it is recently focused in tissue engineering field. The graphene, which can flow electric current, serve as electrical stimulator, too. Moreover, it can emit microelectric current when it is exposed to magnetic or electromagnetic field. The general goal of this doctoral thesis is to fabricate graphene-based platforms, investigate the interaction of nanostructure

and graphene-based nanomaterials, in case of structural, morphological, chemical characteristics, and assess synergic effects by on cell adhesion, cell proliferation, differentiation, and tissue regeneration. Biostimulation-inducing systems on graphene will be also composed and it will be applied on graphene-based nanostructural platforms. Its synergic effects will be thoroughly investigated. First, we combined reduced graphene oxide (RGO) and EMF on osteogenesis and neurogenesis of MSCs. Combination of RGO and PEMFs synergically increased ECM formation, membrane protein, metabolisme, etc. It is expected that the combination of RGO and PEMFs will be an efficient platform for stem cell and tissue engineering. Second, graphene was incorporated into bone cements to reinforce mechanical properties. Owing to the ability that graphene can induce osteogenic differentiation of stem cells, the graphene-incorporated nanocomposite bone cement enhanced osteogenic differentiation. Moreover, the graphene-incorporated nanocomposite bone cement under PEMFs synergically enhanced osteogenic differentiation. Because EMFs can be induced on the implants noninvasively, this system would be applied not only *in vivo* study but also clinical application, resulting in the innovation of regenerative medicine. It can be applicable in clinical study as well as

in vivo study by combining with biodegradable scaffolds. Particularly, EMFs can be exerted on the transplanted scaffolds noninvasively. These systems can be easily applied in clinical study as well as *in vivo* study. Other stimulation systems, electrical, light, etc., have limitations to be applied in *in vivo* study. On the other hand, EMFs stimulation is already commercialized in clinical application. Thus, it is expected that EMFs stimulation system would come true in tissue engineering-based therapy. That would become a turning point in tissue engineering and regenerative medicine.

Keywords

reduced graphene oxide, calcium phosphate cements, pulsed electromagnetic fields, human alveolar bone marrow stem cells, osteogenic differentiation, DNA microarray

Table of Contents

1. Introduction

1.1. Introduction

Tissue engineering is the study to reconstruct tissue and organs of living things by applying material science engineering and biological principles. [1] It is interdisciplinary field that consist of three elements: (1) cells, (2) bio- or physio-chemical factors, and (3) scaffolds. Among them, scaffolds are the substances that cells can reside on or into, which can support cells not only to be adhered and be grown properly, but also become functional tissues. The scaffolds have been made in various forms, e.g. 2-dimensional (2D) film [2], 3-dimensional (3D) platforms [3], bone cements [4], and 3-dimensionally printed platforms. [5] It is of utmost importance that the scaffolds should mimic the nature of tissue and organs to regenerate fully functioned tissues. Because extracellular matrix, a support of cells in native tissues, is composed of nano-sized fibrils or clusters, importance of nanostructure in scaffolds is significantly addressed. [6] It has been reported that according to the change of size, shape, and conformation of nanostructure, cellular adhesion, proliferation, and differentiation can be modulated. [7] In other words, regulation of nanostructure can engineer cellular fate.

Another method to control cellular function is using nanomaterials. For example, incorporating nanomaterials into 2D or 3D polymer-based scaffold is known as one of the easiest way to induce nanostructure and nanotopography in the scaffold. The nanomaterials can derive synergic effects if the nanomaterials have additional functionality. [8] The most preferred functional nanomaterial is carbon nanotube (CNT). [9] Capability to absorb near infrared (NIR) light as well as high conductivity and ultrahigh stiffness of CNT were fascinated by many researchers. [10] Nowadays, graphene is getting spotlight. The graphene, recently discovered in 2004, also have high thermal and electrical conductivity, large specific surface area, and good mechanical properties. [11] Further, it can be functionalized, indicating graphene can be used as diverse forms. Due to those unique characteristics, the graphene have been frequently used in biosensors, drug delivery, and gene delivery but it is recently focused in tissue engineering field. [11] For instance, graphene not only enhanced mechanical properties of scaffolds but also promote osteogenic or neurogenic differentiation of stem cells. [12, 13] The graphene, which can flow electric current, serve as electrical stimulator, too. Moreover, it can emit microelectric current when it is exposed to magnetic or electromagnetic field. [14]

There are four fundamental forces in nature; strong, weak, gravitational, and electromagnetic force. [15] Among them, electromagnetic force is composed of electric and magnetic forces, which can be influenced by each other. [16] The flux of electromagnetic forces can be changed depending on the displacement and the change of electromagnetic force depending on the displacement is called electromagnetic field (EMF). EMF have many subtypes according to frequency, e.g., extremely low frequency-EMF (ELF-EMF), and pulsed EMF (PEMF). Among them, PEMFs are low-frequency fields which have specific amplitudes and wave forms. [17] All lifes living on the Earth is exposed by the magnetic fields ranging from 25 to 65 μT. [18] Expose on EMFs may result in various aspects; Strong irradiation may induce cancers or severe diseases. On contrary, weak irradiation can regenerate damaged tissues or organs. Thus, their biological effects have been investigated for 3 decades. It was reported that EMFs can modulate cell proliferation, DNA replication, wound healing, cytokine expression, and differentiation. [19] Particularly, PEMFs enhanced osteogenic differentiation as well as neurogenic differentiation of mesenchymal stem cells (MSCs). [20] EMFs also enhanced the direct reprogramming of mouse embryonic fibroblast into induced pluripotent stem cells. [21] The

main reason why EMFs can induce biological is that EMF, unlike electric fields (EFs), can easily permeate into cell membranes. [22] EFs can stimulate the receptor of outer membrane. However, It cannot permeate into cell membranes because cell membranes act as capacitors. On contrary, EMFs easily permeate into plasma membrane, that is, it can induce the change of EF of inner cell membrane. The permeated EMFs can induce changes of Ca^{2+} efflux and sequently modulate various biological effects, for instances, growth factor secretion, nitric oxide signaling, mitogen-activated protein kinase (MAPK)/extracellular signal-regulated kinase (ERK), and wnt signaling. [17, 23-27]

Graphene, a two-dimensional crystal of sp^2-hybridized carbon atom, is composed of six-membered rings. [28] Their unique structure made free π electrons that facilitate good electrical conductivity (10^4 S/cm). [29] Furthermore, it has very high elastic modulus (1000 GPa), optical transmittance (97.7%), and thermal conductivity (~5000 W/mK). [30-32] Such electrochemical properties made the graphene being focused on physics, chemistry, materials engineering, and electrical engineering fields. [33] Recently it was focused on cell and tissue engineering because the biological activities of graphene, e.g., good biodegradability, cell adhesion, cellular uptake, and interaction with RNA and DNA, have

been reported. [34] The graphene and its subfamily also improves osteogenesis, neurogenesis, epithelial differentiation, and cardiomyogenic differentiation of stem cells. [35-38] Recently the functionality of graphene is getting a spotlight on the cell and tissue engineering fields. Electrical stimulation-combined graphene was synergically effective on osteogenesis and neurogenesis. [39-40] Its high thermal conductivity is used in curing thermo-responsive hydrogel for cell delivery using near infrared irradiation. [41] However, combination of graphene and EMFs have never been applied in tissue engineering. The free electron residues on outer edge can move owing to the magnetic fields irradiated on graphene, resulting in electric currents flowing through the graphene. [42] Because electric currents generated by the irradiation of EMF can influence on cells together, the synergic effects by electric currents as well as graphene and EMF would enhance the osteogenesis and neurogenesis of MSCs. Moreover, the platform can easily applied in *in vivo* study as well as clinical applications because EMFs can be applied on the implants noninvasively.

Bone cements, which fill in bone defects and rapidly harden inside the defects, are widely used to heal the increasing number of traumatic bone defects due to the aging population. Currently,

polymethylmethacrylates (PMMA) are the most frequently used substance in clinical application because it has *in situ* setting ability and good mechanical properties. [43] However, due to the lack of bioactivity, PMMA cannot be degraded, in other words, they have neither osteoconductivity nor osteoinductivity. Moreover, their high hardening temperature, over 100 degrees, causes necrosis of cells. Although N-butyl-2-cyanoacrylate (BCA) [44] and 2-octylcyanoacrylate (OCA) [45] were developed to resolve this problem, their biological inactiveness remains a critical problem. To complement these weaknesses, calcium phosphate cements (CPCs) were developed. Because CPCs have similar chemical components as native bone, they are bioresorbable, resulting in easy substitution by tissues. They also have good osteoconductivity, osteoinductivity, and low setting temperature. [46] To date, synthetic calcium phosphate (CaP) biomaterials, i.e., hydroxyapatite (HA), dicalcium phosphate (DCP) and α or β-tricalcium phosphate (α or β-TCP) have been utilized as CPCs resources. [47] In addition, natural sources, e.g., sintered animal bones and clamshells, were also used in CPCs due to their similarity with native human bone. These types of CPCs, called natural CPCs, frequently used porcine, [48, 49] bovine, [50], chicken, [51] and horse bone. [52] However, CPCs still have serious problems. Their

mechanical strength is low, which is a critical flaw for use in clinical applications. Thus, many researchers attempt to promote the mechanical strength of CPCs. The mechanical strength of CPCs is deeply related with the micro/nanostructure of the particle size, for instance, porosity, [53] crystal size, [54] powder distribution, [55] and nano/micro CaP particle composition. [56] The addition of additives, e.g., citric acid, [57] cellulose, [58] and fiber [59], significantly improved the mechanical properties, as well. However, because the methods affect CaP synthesis, the additives cannot be used in natural CPCs. Therefore, an easier and more effective method to reinforce the mechanical properties of CPCs should be developed.

Graphene, discovered experimentally in 2004, consists of a two-dimensional (2D) honeycomb lattice structure of carbon. [60] Graphene has many subtypes depending on the fabrication method, for example, graphene made by chemical vapor deposition (CVD), [61] graphene nanoribon (GNR), [62] graphene oxide (GO), [63] and reduced graphene oxide (RGO) [64]. Its good biological properties – interaction with RNA and DNA, cellular adhesion, cellular uptake, antibacterial ability, and good biodegradability - led to its application in the biological field. In tissue engineering, graphene has been used in two ways: 1) stem

cell engineering and 2) strengthening the mechanical properties of scaffolds. First, graphene/GO was involved in osteogenesis, [64] epithelial genesis, [65] and neurogenesis [66] of mesenchymal stem cells (MSCs) and neurogenesis of neural stem cells (NSCs). [67] Furthermore, GO-CaP nanocomposite synergically enhanced osteogenic differentiation of MSCs. [68] Secondly, graphene has been used to enhance the mechanical properties of tissue-engineered scaffolds. Yang et al. reported that the elastic modulus and maximum tensile strength were enhanced by the addition of GO. [69] Baradaran et al. and Fan et al. also reported that the mechanical strength of HA-RGO and HA-GO nanocomposites was improved compared with HA composite. [70, 71] These two properties – acceleration of osteogenic differentiation and reinforcement of mechanical strength – can also be utilized in natural CPCs.

If nanomaterials, especially graphene, are combined on scaffolds, synergistic effects in cell function and tissue regeneration can be estimated. Those scaffolds can induce structural and biostimulative cues simultaneously if graphene-derived stimulation-inducing systems are constructed. The system which can provoke biostimulation via graphene will advance the synergic effects of nanostructure and graphene-based nanomaterials. Thus, the general goal of this doctoral thesis is to

fabricate graphene-based nanostructural platforms, investigate the interaction of nanostructure and graphene-based nanomaterials, in case of structural, morphological, chemical characteristics, and assess synergic effects by on cell adhesion, cell proliferation, differentiation, and tissue regeneration. Biostimulation-inducing systems on graphene will be also composed and it will be applied on graphene-based platforms. Its synergic effects will be thoroughly investigated.

First, we combined graphene and EMF on osteogenesis and neurogenesis of MSCs. (Fig. 1.1) As a graphene substrata, reduced graphene oxide (RGO) were coated on Glass coverslips. Among EMFs, PEMF was used due to its well-known efficacy on osteo- and neurogenesis of MSCs. At first, the characteristics of RGO were analyzed. Their chemical properties were measured by X-ray photoelectron spectroscopy (XPS), X-ray diffraction (XRD), and raman spectroscopy and its magnetic properties were analyzed. After evaluation, the RGO were adsorbed on glass and its morphological and electrical properties were investigated. Then, *in vitro* study was conducted using human alveolar bone marrow stem cells (hABMSCs) exfoliated from mandible. Their cell viability, cell adhesion, and ECM formation by RGO and PEMFs were assessed. After that, their osteogenic capability was studied

by alkaline phosphatase (ALP) activity study, immunocytochemistry (ICC), reverse transcription polymerase chain reaction (RT-PCR), alizarin red staining (ARs), and von Kossa staining (VKs). Their neurogenic as well as chondrogenic and adipogenic capability was also studied. Moreover, microarray was conducted to reveal the mechanism of RGO and PEMFs on osteogenic and neurogenic differentiation.

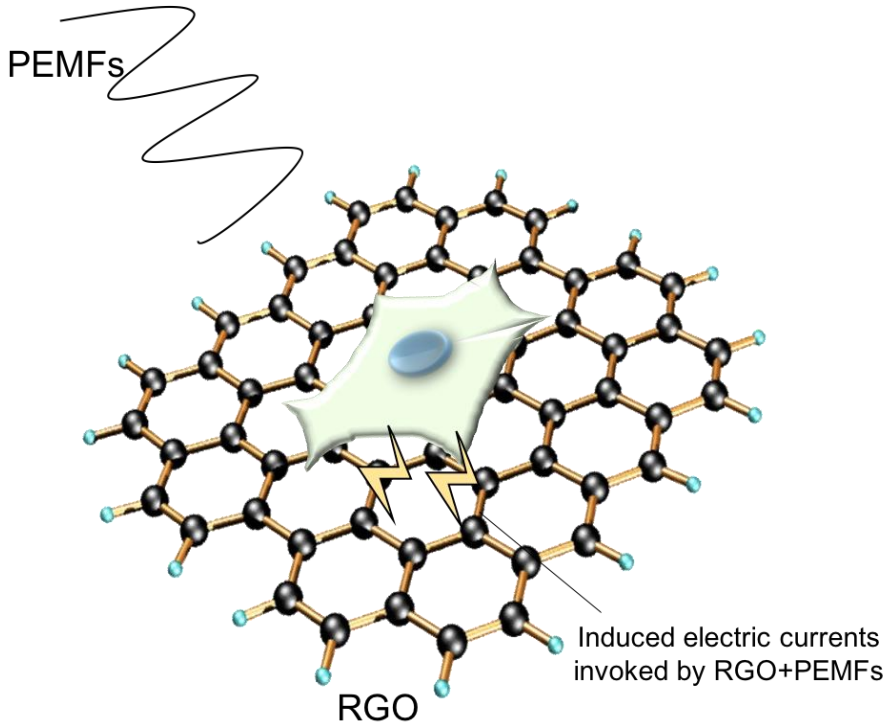

Fig. 1.1. Schematic diagram of the research concept of part II. HABMSCs adhere on RGO substrates. PEMFs were exerted on the cell-cultured RGO substrates. Not only PEMFs, induced electric currents generated on RGO due to PEMFs would also result in synergic effects on the behavior of hABMSCs.

Second, we hypothesized that if we incorporate graphene in natural CPCs, we could reinforce the mechanical properties as well as the osteoinductivity of natural CPCs. (Fig. 1.2) Therefore, we fabricated graphene-incorporated natural CPCs and evaluated their various properties. As a graphene ingredient, RGO was chosen because of its several advantages – easy synthesis and easy incorporation. At first, their characteristics, e.g., morphology, chemical composition, and mechanical properties, were analyzed. *In vitro* study was conducted using a murine osteoblast cell line (MC3T3-E1) and rat-derived adipose stem cells (rASCs). Their cytotoxicity, viability, and adhesion were analyzed. Then, a migration assay was assessed to verify the osteoconductivity. Finally, their osteogenic differentiation was evaluated by western blot analysis, ICC, and ARS, suggesting that RGO-reinforced CPC (RGO-CPC) is a promising tool for clinical application.

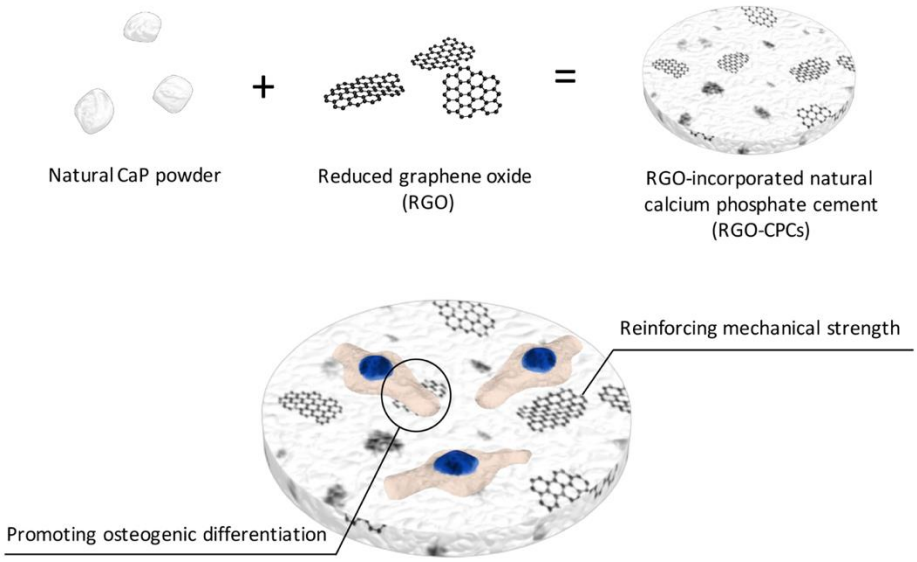

Fig. 1.1. Schematic diagram of the research concept of part I. Natural CaP powder and RGO were thoroughly mixed. Then, the mixed powder was hardened by CS solution to fabricate RGO-CPCs. The RGO in RGO-CPCs is expected to reinforce the mechanical properties and improve osteogenic differentiation, which would contribute to better bone regeneration.

1.2. Objectives

It is the driving force of this research that the combination of nanostructure and nanomaterials may have synergic effects and influence on the scaffold configuration, cell function, and tissue regeneration. Therefore, in this study, the scaffolds that have nanostructure and graphene-based nanomaterials simultaneously will be fabricated and their unique properties will be investigated. Then, they will be utilized in tissue engineering. Biostimuli-inducing graphene based system will be fabricated and investigated, too. Finally, these developed scaffolds will be used in *in vivo* study and be examined for tissue regeneration. Detailed goal is as follow:

Aim 1: To fabricate nanomaterial-based nanostructural scaffold (nanofibrous 2D scaffolds, nanocomposite bone cements, etc.)

Aim 2: To investigate the relation between nanostructure and nanomaterials, especially in the structure, conformation and chemical binding

Aim 3: To assess the synergic effects of nanostructure and nanomaterials on cell function, e.g. cell adhesion, cell viability, differentiation, commitment, and tissue regeneration

Aim 4: To build systems that can provoke biostimulation via graphene and apply it to graphene-based platforms.

2. Literature Review: Regulation of Stem Cell Behaviors by Graphene-Based Platforms

2.1. Introduction

Stem cells are characterized by their unique abilities to reproduce themselves (i.e., self-renew) and differentiate into various tissue types of cells, and stem cell-based therapies have been recognized as a promising new approach for various disease treatments including tissue regeneration [73-77]. Stem cells reside within instructive and tissue-specific niches in the body, such as complex and controlled biochemical mixtures of soluble or insoluble factors, as well as extracellular communication via direct or indirect cell-cell communication [73,78-79]. It has been known that these complex microenvironments can strongly affect the stem cell function [73-81]. In particular, it is widely accepted that stem cells display high sensitivity to the local topographies or chemical compositions of extracellular matrix (ECM) which was typically composed of complex and well-defined nanostructures of protein fibers such as fibrillar collagens and elastins with feature sizes ranging from tens to several hundreds of nanometers [78-80]. In conjunction with these aspects, it is important to develop a synthetic ECM to regulate or improve stem cell functions for stem

cell-based therapies toward better clinical applications of stem cells [73-80].

Carbon-based nanomaterials have been considered as one of interesting sources to develop synthetic ECMs as a stem cell platform due to their unique physicochemical properties (Fig. 2.1) [81-82]. For example, carbon nanotubes (CNTs), one of the representative carbon-based nanomaterials, have been extensively studied for a variety of applications for stem cells because of their unique dimension structures [81-83] although their extreme one-dimensional morphology is found to be somewhat cytotoxic [84]. On the other hand, it is expected that graphene, the most recently discovered new carbon-based nanomaterial, may provide better biocompatibility than other carbon-based nanomaterials because of the two-dimensional mild shape [84]. In particular, its similar properties in terms of physical structure and chemical composition of native ECMs as well as remarkable mechanical and electrical conductible properties has gained tremendous attentions as a new material for stem cell culture platforms or scaffolds [80,84]. Furthermore, graphene has many advantages to develop effective stem cell culture platforms; for example, (1) it is easy to modify the surface of graphene with various functionalization methods, (2) graphene can

reinforce the mechanical property of organic or inorganic platforms, and (3) the high conductivity of graphene can be used as an effective biocompatible electrode for electro-active stem cells [81,84].

Here, we review graphene-based platforms for stem cell culture platforms and discuss how the engineered graphene platforms can be used to regulate or improve the function of stem cells. In particular, we focus on the most recent efforts to investigate the effects of these platforms on cytotoxicity, adhesion, proliferation, and differentiation of stem cells. We also highlight the possible mechanism on the controlled stem cell behavior by cell-graphene interactions as well as strategies to use graphene-based platforms for advanced stem cell-based therapy.

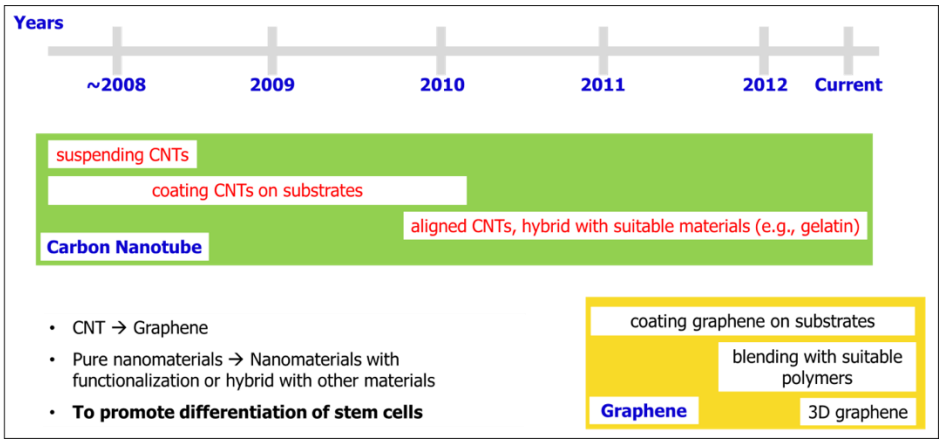

Fig. 2.1. Research trend on the carbon nanotube and graphene as representative carbon-based nanomaterials for stem cell engineering.

2.2. Graphene-Based Platforms

2.2.1. Graphene

Graphene is a flat monolayer of carbon atoms closely packed into a honeycomb shaped 2-dimensional lattice, and its unique nanotopography has gained tremendous attentions as new stem cell culture platforms or scaffolds [84-85]. It is known that graphene have a lateral dimension of about 8 to 10 nm and a height displacement of about 0.7 to 1 nm. In addition, it is reported that the properties of graphene are different according to the synthesis methods. For example, graphene which is chemically exfoliated from oxidized graphite has oxygen containing hydrophilic functional groups (called as ‘graphene oxide (GO)’) whereas graphene synthesized by chemical vapor deposition (CVD) has hydrophobic and flexible properties [84].

2.2.2. Graphene-based platforms for stem cells

For the past years, various graphene-based platforms have been developed and used for controlling or improving stem cell behaviors (Table 2.1). First of all, two- dimensional (2D) graphene films were first used for enhancing stem cell differentiation [87]. The CVD graphene

films were transferred on substrates (e.g., glass) [87]. On the other hand, the GO films were coated on substrates using using a self-assembly method (i.e., using electrostatic interaction between negatively charged GOs and positively charged substrates) [88].

Three-dimensional (3D) graphene foams were synthesized by CVD method using Ni foam template for stem cells and tissue engineering applications [89]. The 3D graphene forms showed porous and interconnected structures even though they were constructed by few-layer or multi-layer graphene sheets [89]. In particular, they showed interesting properties such as the porosity of about 99% and pore size of about 100–300 μm [89]. In addition, it was observed that the graphene layers in 3D graphene were extremely thin, but the network possessed excellent mechanical strength and flexibility, and can stand alone [89]

Moreover, graphene-incorporated platforms were reported to promote functions of stem cells [90]. For example, reduced graphene oxide (RGO)–chitosan films were fabricated after spin-coating of the RGO–chitosan composite solutions on glass [91]. Interestingly, the RGO–chitosan films showed transparent properties and nanodot-like nanotopography while various layers of RGO were occasionally observed in the RGO–chitosan films.

In summary, for the past few years, CVD, GO, or RGO films, 3D graphene foams, and graphene-incorporated polymer platforms have been developed for stem cell engineering, particularly for improving differentiation of stem cells.

Table 2.1. Graphene-based platforms for stem cells

Platform Characteristics					Applications		Ref.
Dimension	Type	Platforms	Fabrication	Target Cell Type	Advantages	Potential use	
1D	GNR	Suspension of GNR	Reduction from GONR	hUCBMSCs	Low toxicity in low concentration Possibility to modify surfaces	Gene delivery	Akhavan et al.
	rGO	Suspension of rGO platelet	Modified Hummer's method	hUCBMSCs	Low toxicity in large particle size Possibility to modify surfaces	Gene delivery	Akhavan et al.
2D	GO	Coated on PDMS	Hummer's method	hBMSCs	Enhanced osteogenesis	Cell culture platform	Lee et al.
			Attached on gold electrode	HBLF3	Good detection of cell proliferation	Cell Chip	Kang et al.
		Coated on Coverslip	Coating APTES before GO coating	iPSCs	Enhanced proliferation	Cell culture platform	Chen et al.
			Coating APTES before GO coating	hASCs	Enhanced osteogenic, adipogenic, and epithelial differentiation	Cell culture platform	Kim et al.
		Adsorption of GONR on PDMS	Oxidazing MWCNT	hUCBMSCs	Nanotopography fabrication	Cell culture platform	Akhavan et al.
	rGO	Coated on Coverslip	Immerse GO coating in DMF	iPSCs	Enhanced proliferation	Cell culture platform	Chen et al.
		Adsorption of rGONR on PDMS	Reduction from GONR	hUCBMSCs	Applying of nanotopography	Cell culture platform	Akhavan et al.
		rGO-chitosan substrata	Spin coating of rGO-chitosan composite	hASCs	Fabrication Nanotopography	3D culture platform Tissue engineering	Kim et al.
	CVD Graphene	Coated on Glass	CVD on copper foil	hMSCs	Enhanced osteogenesis	Cell culture platform	Nayak et al.
			CVD on copper foil	hNSCs	Enhanced neurogenesis	Cell culture platform	Park et al.
		Coated on Si/SiO2	CVD on copper foil	hMSCs	Enhanced osteogenesis	Cell culture platform	Nayak et al.
		Coated on PET	CVD on copper foil	hMSCs	Enhanced osteogenesis	Cell culture platform	Nayak et al.
		Coated on PDMS	CVD on copper foil	hMSCs	Enhanced osteogenesis	Cell culture platform	Nayak et al.
			CVD on copper foil	hBMSCs	Enhanced osteogenesis	Cell culture platform	Lee et al.
	Functionalized Graphene	Fluorinated Graphene Sheet	Exposing to XeF_2	hBMSCs	Enhanced surface charge	Cell culture platform	Wang et al.
		Wrinkled GO sheet	functionalizing GO sheets with methacrylate groups	hBMSCs	Enhanced osteogenics differentiation	Cell culture platform	Tang et al.
3D	CVD graphene	Multilayer Graphene Foam	Grown on 3D Ni scaffolds	hBMSCs	Enhanced osteogenic differentiation	Bone Tissue engineering	Crowder et al.
				hNSCs	Enhanced proliferation and neural differentiation	Nerve Tissue engineering	Li et al.

2.3. Stem Cell Behaviors on Graphene-Based Platforms

In this section, we describe the efforts on regulating the stem cell behaviors by using graphene-based platforms so far.

2.3.1. Cytotoxicity of Grapyhene in Stem Cells

We first discuss the cytotoxicity of graphene in stem cells. Despite the great potential graphene holds for stem cell and tissue engineering, the in-depth study about cytotoxicity of graphene in stem cells has been not reported well (Table 2.2). The recent study has reported that low concentrations (less than 0.1 mg/mL) of GO did not show cytotoxicity in hMSCs, while while high concentrations (greater than 0.1 mg/mL) were somewhat cytotoxic to hMSCs when the hMSCs were cultured on the tissue culture dish with medium containing RGO [90]. On the other hand, many reports have reported that graphene-based platforms (e.g., graphene film, 3D graphene foam) showed very good cell viability [87,89]. Thus it is strongly needed to perform the in-depth study on otoxicity of graphene in stem cells *in vitro* and *in vivo*.

Table 2.2. Cytotoxicity of graphene-based platforms in stem cells. The ‘o’ indicates the control value (uncoated graphene substrate).

Variety of graphene-based platforms				Application for stem cell behaviors	Ref.
Dimension	Type	Platforms	Target Cell Type	Cytotoxicity	
1D	rGONR	Suspension of GNR	hUCBMSCs	0~2 (increase as concentration increase)	Akhavan et al.
	rGO platelet	Suspension of rGO platelet	hUCBMSCs	0~2 (increase as grapheme size decrease)	Akhavan et al.
	GO pellet	Suspension of GO pellet	HBI.F3	0~2 (increase as grapheme size decrease)	Kang et al.
2D	GO	Coated on PDMS	hBMSCs	Not performed	Lee et al.
		Coated on Coverslip	iPSCs	Not performed	Chen et al.
			hASCs	0~1 (increase as concentration increase)	Kim et al.
		Adsorption of GONR on PDMS	hUCBMSCs	Not performed	Akhavan et al.
	rGO	Coated on Coverslip	iPSCs	Not performed	Chen et al.
		Adsorption of rGONR on PDMS	hUCBMSCs	Not performed	Akhavan et al.
		rGO-chitosan substrata	hASCs	Not performed	Kim et al.
	CVD Graphene	Coated on Glass	hMSCs	Not performed	Nayak et al.
			hNSCs	Not performed	Park et al.
		Coated on Si/SiO2	hMSCs	Not performed	Nayak et al.
		Coated on PET	hMSCs	Not performed	Nayak et al.
		Coated on PDMS	hMSCs	Not performed	Nayak et al.
			hBMSCs	Not performed	Lee et al.
	Functionalized Graphene	Fluorinated Graphene Sheet	hBMSCs	Not performed	Wang et al.
		Wrinkled GO sheet	hBMSCs	Not performed	Tang et al.
3D	CVD graphene	Multilayer Graphene Foam	hBMSCs	Not performed	Crowder et al.
			hNSCs	Not performed	Li et al.

2.3.2. Adhesion of Stem Cells on Graphene-Based Platforms

The general behavior of stem cell can be characterized with following steps: adhesion on a substrate spreading cytoskeleton development (cell shape) functions (e.g., proliferation and differentiation). Therefore, the adhesion of stem cells on substrates may be a fundamental and important requirement for regulating stem cell functions.

Some studies have investigated the adhesion of stem cells on the graphene-based platforms (**Table 2.3**). Lee et al., reported that CVD graphene or GO films enhanced the initial adhesion of human mesenchymal stem cells hMSCs on the substrates compared to that on PDMS [91]. Chen et al., reported that CVD graphene or GO films promoted the initial adhesion of induced pluripotent stem cells (iPSCs) than glass [92]. They also showed that GO filmss are better than CVD graphene films in case of the adhesion of iPSCs [92]. Recently, Kim et al., reported that GO film influenced the adhesion of human adipose tissue-derived stem cells (hASCs) although the GO film did not greatly influence the attachment of hASCs compared to the uncoated GO substrate [88]. Interestingly, they showed that the GO film significantly influenced the focal adhesions (FAs) of the hASCs on the substrates as well as higher correlation between the orientations of the actin filaments

and vinculin bands in the hASCs cultured on the GO films than on the uncoated GO substrates [88]. In addition, it was reported that the GO films have the higher cell affinity under fluid shear stress, compared to glass (uncoated GO) [88]. Furthermore, it was reported that the graphene influence the shape of stem cells. For example, hMSCs showed the spindle shape morphology on the CVD graphene films while the morphology of hMSCs showed the polygonal shape on the SiO_2 substrates [93].

Table 2.3. Adhesion of graphene-based platforms in stem cells. The ‘o’ indicates the control value (uncoated graphene substrate).

Variety of graphene-based platforms				Application for stem cell behaviors	Ref.
Dimension	Type	Platforms	Application to	Adhesion	
1D	rGONR	Suspension of GNR	hUCBMSCs	Not performed	Akhavan et al.
	rGO platelet	Suspension of rGO platelet	hUCBMSCs	Not performed	Akhavan et al.
	GO pellet	Suspension of GO pellet	HBI.F3	Not performed	Kang et al.
2D	GO	Coated on PDMS	hBMSCs	1	Lee et al.
		Coated on Coverslip	iPSCs	2	Chen et al.
			hASCs	0	Kim et al.
		Adsorption of GONR on PDMS	hUCBMSCs	Not performed	Akhavan et al.
	rGO	Coated on Coverslip	iPSCs	0	Chen et al.
		Adsorption of rGONR on PDMS	hUCBMSCs	Not performed	Akhavan et al.
		rGO-chitosan substrata	hASCs	0	Kim et al.
	CVD Graphene	Coated on Glass	hMSCs	1	Nayak et al.
			hNSCs	1	Park et al.
		Coated on Si/SiO2	hMSCs	1	Nayak et al.
		Coated on PET	hMSCs	1	Nayak et al.
		Coated on PDMS	hMSCs	1	Nayak et al.
			hBMSCs	1	Lee et al.
	Functionalized Graphene	Fluorinated Graphene Sheet	hBMSCs	1	Wang et al.
		Wrinkled GO sheet	hBMSCs	0~2 (increase as topology increase)	Tang et al.
3D	CVD graphene	Multilayer Graphene Foam	hBMSCs	Not performed	Crowder et al.
			hNSCs	Not performed	Li et al.

2.3.3. Proliferation of Stem Cells on Graphene-Based Platforms

One of the major issues of stem cell-based therapy in clinical applications is to obtain an abundance of stem cells with multipotent ability due to difficulty on maintaining the multipotency in stem cells. It has been reported that graphene-based platforms provide suitable environment for proliferation of stem cells (Table 2.4). Lee et al., reported that GO films increased the proliferation of hMSCs compared to PDMS (uncoated GO) [91]. Kim et al., reported that the proliferation of hASCs on GO films were similar to that on the glass or the normal tissue culture dish [88]. Interestingly, Chen et al., reported that the GO films increased the proliferation of iPSCs than the glass [92]. In addition, recent study showed that the 3D graphene foams promoted the proliferation of human neural stem cells (hNSCs) that 2D CVD graphene [89]. Together, these studies suggest that the graphene-based platforms may be suitable for the proliferation of stem cells although a detailed study should be performed to verify the multipotency of proliferated stem cells on them.

Table 2.4 Proliferation of graphene-based platforms in stem cells. The ‘o’ indicates the control value (uncoated graphene substrate).

Variety of graphene-based platforms				Application for stem cell behaviors	Ref.
Dimension	Type	Platforms	Application to	Proliferation	
1D	rGONR	Suspension of GNR	hUCBMSCs	Not performed	Akhavan et al.
	rGO platelet	Suspension of rGO platelet	hUCBMSCs	Not performed	Akhavan et al.
	GO pellet	Suspension of GO pellet	HBI.F3	Not performed	Kang et al.
2D	GO	Coated on PDMS	hBMSCs	1	Lee et al.
		Coated on Coverslip	iPSCs	2	Chen et al.
			hASCs	0	Kim et al.
		Adsorption of GONR on PDMS	hUCBMSCs	2 (higher than GO sheets)	Akhavan et al.
	rGO	Coated on Coverslip	iPSCs	0	Chen et al.
		Adsorption of rGONR on PDMS	hUCBMSCs	2 (higher than rGO sheets)	Akhavan et al.
		rGO-chitosan substrata	hASCs	0	Kim et al.
	CVD Graphene	Coated on Glass	hMSCs	0	Nayak et al.
			hNSCs	1	Park et al.
		Coated on Si/SiO2	hMSCs	0	Nayak et al.
		Coated on PET	hMSCs	0	Nayak et al.
		Coated on PDMS	hMSCs	0	Nayak et al.
			hBMSCs	1	Lee et al.
	Functionalized Graphene	Fluorinated Graphene Sheet	hBMSCs	2	Wang et al.
		Wrinkled GO sheet	hBMSCs	0~2 (increase as topology increase)	Tang et al.
3D	CVD graphene	Multilayer Graphene Foam	hBMSCs	-1	Crowder et al.
			hNSCs	3	Li et al.

2.3.4. Differentiation of Stem Cells on Graphene-Based Platforms

One of the major issues of the use of graphene-based platforms is to regulate or improve the stem cell differentiation (Table 2.5). Several studies reported an accelerated osteogenic differentiation of hMSCs on graphene substrates. For example, Ozyilmaz et al., reported that the CVD graphene film greatly accelerated osteogenesis of hMSCs [87]. On the other hand, the rate of osteogenic differentiation induced by graphene film was similar to that induced by BMP-2 [87]. Part et al., reported that the CVD graphene film could contribute better adhesion of both glial cells and undifferentiated hNSCs as well as induce the differentiation of hNSCs into neurons on graphene [94]. The multiple differentiation study of hASCs was performed by Kim et al. [88]. The enhanced differentiation of hASCs included osteogenesis, adipogenesis, and epithelial genesis, while chondrogenic differentiation of hASCs was decreased, compared to tissue culture polystyrene as a control substrate.

Wang et al., fabricated fluorinated graphene film and showed that the enhanced neurogenesis of hMSCs [95]. In particular, they also tried to modify the graphene films by printing PDMS barriers directly, which showed the alignment of hMSCs to induce the neurogenesis of hMSCs [95].

As for an example for 3D graphene scaffolds for enhancing stem cell differentiation, Li et al., reported that 3D graphene scaffolds could enhance the NSC differentiation towards astrocytes and especially neurons as well as good electrical coupling of 3D graphene scaffolds with differentiated NSCs [89].

Table 2.5 Differentiation of graphene-based platforms in stem cells. The 'o' indicates the control value (uncoated graphene substrate).

Differentiation	Dimension	Type	Platforms	Cell Source	Chemical inducer	Degree of Differentiation	Specifications	Ref.
Osteogenesis	2D	CVD Graphene	Coated on Glass	hMSCs	+	1	Slightly enhanced compared to control	Nayak et al.
					_	3	Almost same results compared with chemical inducers	Nayak et al.
			Coated on Si/SiO2	hMSCs	+	1	Slightly enhanced compared to control	Nayak et al.
					-	3	Almost same results compared with chemical inducers	
			Coated on PET	hMSCs	+	1	Slightly enhanced compared to control	Nayak et al.
					-	3	Almost same results compared with chemical inducers	
			Coated on PDMS	hMSCs	+	1	Slightly enhanced compared to control	Nayak et al.
					-	3	Almost same results compared with chemical inducers	
				hBMSCs	+	2	Higher adsorption of chemical inducer on graphene sheet	Lee et al.
		Graphene Oxide	Coated on PDMS	hBMSCs	+	1	Lower adsorption of chemical inducer on graphene sheet	Lee et al.
			Coated on coverslips	hASCs	+	1	Stiffness may influence on osteogenesis	Kim et al.
			Graphene oxide nanogrid on PDMS	hUCBMSCs	+	3	Influence of nanotopography on osteogenesis	Akhavan et al.
					-	2	Higher than GO sheet	
		Reduced Graphene oxide	Graphene nanogrid on PDMS	hUCBMSCs	+	4	Influence of nanotopography on osteogenesis	Akhavan et al.
					-	2	Higher than rGO sheet	
			Graphene-chitosan substrata	hASCs	-	2	Osteogenesis without chemical inducers	Kim et al.
					+	1	Less effective when chemicals induced	
		Functionalized graphene	Wrinkled GO sheet	hBMSCs	+	3	More roughness, more osteogenesis	Tang et al.
	3D	CVD Graphene	Multilayer graphene foam	hBMSCs	-	1	3D structure may influence despite of absence of chemical inducer	Crowder et al.
Adpogenesis	2D	CVD Graphene	Coated on PDMS	hBMSCs	+	0	Lower adsorption of chemical inducer on graphene sheet	Lee et al.
		Graphene Oxide	Coated on PDMS	hBMSCs	+	2	Higher adsorption of chemical inducer on graphene sheet	Lee et al.
			Coated on coverslips	hASCs	+	2	Adsorption of chemical inducer may affect	Kim et al.
Neurogenesis	2D	CVD Graphene	Coated on Glass	hNSCs	+	2	Neuronal function increased	Park et al.
		Reduced Graphene oxide	Graphene-chitosan substrata	hASCs	+	2	Enhanced cell adhesion and cell-cell connection may affect	Kim et al.
		Functionalized Graphene	Fluorinated Graphene on PDMS	hNSCs	+	2	Enhanced surface charges	Wang et al.
	3D	CVD Graphene	Multilayer graphene foam	hBMSCs	-	0	Neurogenesis is not enhanced	Crowder et al.
				hNSCs	+	2	Neural function is observed	Li et al.
Chondrogenesis	2D	Graphene Oxide	Coated on coverslips	hASCs	+	-2	Stiffness may be negatively effective	Kim et al.
Epithelal genesis	2D	Graphene Oxide	Coated on coverslips	hASCs	+	2	Enhanced epithelal differentiation	Kim et al.

2.3.5. Mechanism for Regulating Stem Cell Behaviors by Graphene-Based Platforms

The mechanisms underlying the effects of the graphene-based platforms on stem cells behaviors such as adhesion, proliferation, and differentiation remain unknown well. It is usually hypothesized a combination of factors including nanoscale structure, strong stiffness, roughness, reactive oxygen functional groups, and absorption of biomolecules. It was reported that the surface oxygen content of a GO film has a great influence on the behaviors of osteoblasts, fibroblasts, and myoblasts in which the oxygen functional groups on GO films introduced a negatively charged surface, which led to various interactions such as electrostatic forces, hydrogen bonding, and hydrophobic interactions between the GO film and cells as well as specific proteins absorption [88]. In addition, Lee et al. [89] reported that CVD graphene or GO films influenced the specific proteins absorption related in differentiation of stem cells (Figs. 2.15 and 16) [91].

Recently, it was observed that the incorporated graphene in chitosan substrata could influence initial cell adhesion and interaction between cell–cell or cell–substrate, which might be another possible explanation to enhance the differentiation of hMSCs on the RGO–chitosan substrata (Fig. 2.17) [90]. Taken together, although the further

study is strongly needed, the graphene may influence the protein absorption on the surface of platform, which may be able to influence the adhesion and shape to regulate function of stem cells.

2.4. Summary and Outlook

Graphene-based platforms have demonstrated as an effective strategy for adhesion, proliferation, and differentiation of stem cells. The unique nanostructure as well as the modified physicochemical property such as surface functionalization or surface roughness of graphene-based platforms could regulate or improve the behaviors of stem cells. On other hand, it is also true that most studies so far have focused on the interaction between stem cells and graphene-based platforms in *in vitro* study. Here, we discuss the other challenges and future works using graphene for stem cells as follows; (1) it is strongly needed to perform in-depth study on the *in vitro* and *in vivo* biocompatibility to be acceptable for FDA approval to use graphene-based platforms toward their clinical applications; (2) the synergistic effects of graphene-based platforms with other factors such as chemical, physical, electrical cues for stem cell engineering may give us other opportunities to improve the stagey to use graphene for stem cells; (3) it is also needed to conduct out the mechanism study including signaling pathway how graphene could promote the differentiation of stem cells, which will allow us to realize how we can use the graphene-based platforms as a tool for advanced stem cell and tissue engineering applications.

3. Part Ⅰ: Pulsed Electromagnetic Fields-Assisting Reduced Graphene Oxide Substrata for Multidifferentiation of Human Stem Cells

3.1. Materials and Methods

3.1.1. Preparation and Characterization of RGO

GO was produced by a modified Hummers method.[35] Briefly, graphite powders (Alfa Aesar graphite powder, universal grade, 200 mesh, 99.9995%) were stirred into $NaNO_3$ and H_2SO_4 while being cooled in an ice water bath for 4 h. $KMnO_4$ was gradually added and the mixture was stirred at 25℃ until a highly viscous liquid was obtained. Deionized water was added and the suspension was heated in a water bath at 98 C for 15 min. The suspension was further treated with warm water and H_2O_2 in sequence. The mixture was centrifuged at least five times at 4000 rpm and washed with HCl and water. GO was dried at 50℃ for 24 h. The resulting homogeneous dispersion (100 mL) was mixed with 1 mL of hydrazine solution (35 wt% in water) and 7 mL of ammonia solution (28 wt% in water). RGO powder was then obtained by filtration and drying in vacuum. The presence of crystalline phases on the RGO

was detected by XRD and Raman spectroscopy. In XRD, an X-ray diffractometer (New D8 advanced XRD, Bruker, Germany) with copper Kα radiation at 40 kV and 40 mA was used. The Raman spectra was obtained with a T64000 (Horiba Jobin Yvon) at an excitation wavelength of 514.54 nm. XPS was conducted on a Sigma Probe (ThermoVG, U.K) operating at a base pressure of 5 × 10 − 10 mbar at 300 K with a nonmonochromatized Al K α line at 1486.6 eV, a spherical sector analyzer of 180 °, a mean diameter of 275 mm, an analysis area of 15 μm to 400 μm, and multichannel detectors. The magnetometry of RGO was measured by physical property measurement system (PPMS®, Quantum Design Inc., San Diego, CA, USA). Measured temperature was 289.7K and the range of magnetic field was ±0.15 μT.

3.1.2. Preparation and Characterization of RGO Substrates

In total, 12- or 24-well sized bare glass substrates were cleaned with acetone and isopropyl alcohol for 3 min in an ultrasonic bath, followed by cleaning with deionized water. Piranha treatment was also performed to remove the rem- nant dirt. The substrates were treated in a toluene solution containing 10 mM 3-aminopropyltriethoxysilane (APTES) for 2 h. Then, the substrates were washed with toluene and

ethanol, followed by cleaning with de-ionized water and drying in a stream of nitrogen. For the fabrication of GO thin films, the substrates were immersed in a 2 mg/mL GO aqueous suspension for 2 h, washed with ethanol and deionized water, and dried in a stream of nitrogen. The resulting substrates were mixed with 1 mL of hydrazine solution (35 wt% in water) and 7 mL of ammonia solution (28 wt% in water). RGO powder was then obtained by filtration and drying in vacuum. The fabricated RGO substrates were observed by optical microscope (Ti-E, Nikon, Japan) and field-emission scanning electron microscope (FESEM; SUPRA 55VP, Carl Zeiss, Germany).

3.1.3. Cell Culture and Induction of PEMFs

hABMSCs were collected at the Intellectual Biointerface Engineering Center, Dental Research Institute, College of Dentistry, Seoul National University. Cells were cultured in α-minimum essential medium (MEM) containing 10% fetal bovine serum (FBS, Welgene Inc., Republic of Korea), 10 mM ascorbic acid (L-ascorbic acid), antibiotics, and sodium bicarbonate at 37° C in a humidified atmosphere of 5% CO_2 (Steri-Cycle 370 Incubator, Thermo Fisher Scientific. USA). The medium was changed every other day. When the cells became confluent,

they were detached with 1 mL trypsin-EDTA, counted, and passaged. The cells were passaged before reaching confluence and used at between 5 or 6 passages. For an *in vitro* study, four groups were chosen: 1) Glass, the group cultured on glass substrates as control; 2) Glass+PEMFs, the group cultured on glass substrates and irradiated by PEMFs; 3) RGO, the group cultured on RGO subtrates; 4) RGO+PEMFs, the group cultured on RGO substrates and irradiated by PEMFs. PEMFs stimulation condition was following our previous study. **Lim 2013** Briefly, the PEMFs were irradiated using a solenoid, (Fig. 2A) Electric signals, of which condition was square wave, ±5 V, 50 Hz-frequency, and 50%-duty cycle, were generated using a function generator. The condition of resultant PEMFs was 0.6 ± 0.05 mT with 50 Hz and expose time on samples was 30 min/day.

3.1.4. Cell Proliferation and Viability Test.

Cell viability was measured by WST-1 assay (EZ-Cytox cell viability assay kit, Daeillab Service Co., LTD). Watersoluble formazan was quantifed by a multiwell spectrophotometer (Victor 3, Perkin Elmer, USA), measured at 450 nm. DNA concentration was quantified by CyQUANT cell proliferation assay kit (Invitrogen) and the λ DNA

standard (Invitrogen) following manufacture's protocols. For ICC, hAMBSCs (1×10^4 cells/sample) were seeded on the substrates, and allowed to spread for 7 days in culture media at 37℃ in a humidified atmosphere containing 5% CO_2. Adhered cells were fixed with a 4% paraformaldehyde solution (Sigma-Aldrich, Milwaukee, WI) for 20 min, permeabilized with 0.2% Triton X- 100 (Sigma-Aldrich, WI, Milwaukee) for 15 min, and stained with TRITC-conjugated phalloidin (Millipore, Billerica, MA) and 4, 6-diamidino-2-phrnykinodole (DAPI; Millipore, Billerica, MA) for 1 h. Focal adhesions (FAs) were stained with a monoclonal anti-vinculin antibody (1:100; Millipore, Billerica, MA) and an FITC-conjugated goat anti-mouse secondary antibody (1:500; Millipore, Billerica, MA). Fibronectin was stained with a monoclonal anti-fibronectin antibody (1:100; Millipore, Billerica, MA) and an FITC-conjugated goat anti-rabbit secondary antibody (1:500; Millipore, Billerica, MA). Images were taken using a confocal laser scanning microscope (LSM710, Carl Zeiss, Germany).

3.1.5. Osteogenic Differentiation

HABMSCs were placed at a density of 1.0×10^4 cells/cm^2 and cultured for about 1 and 2 weeks in α -MEM containing 10 μM

dexamethasone (Sigma-Aldrich, WI, Milwaukee), 50mM β -glycerophosphate (Sigma-Aldrich, WI, Milwaukee) and 50 μ g/mL ascorbic acid (Sigma-Aldrich, WI, Milwaukee). The induction culture medium was changed every second or third day. ALP activity was quantified on week 1 using SensoLyte^{TM} ALP Assay kit (AnaApec, USA) following manufacturer's guide. RT-PCR was conducted on week 2. Total RNA was isolated with Trizol reagent (Invitrogen, USA) and used to synthesize cDNA using a first-strand cDNA synthesis kit (Invitrogen, USA) according to the instructions of the manufacturer. The primer information is listed in Table 2. The products were separated by electrophoresis on a 1 % agarose gel and visualized by ultraviolet induced fluorescence. ICC was conducted on week 2 to exhibit the expression of OPN. The cultured cells were washed in phosphate buffered saline (PBS, Sigma-Aldrich, Milwaukee, WI, USA), fixed in a 4% paraformaldehyde solution (Sigma-Aldrich, Milwaukee, WI, USA) for 20 min, and permeabilized with 0.2% Triton X-100 (Sigma-Aldrich, WI, Milwaukee, USA) for 15min. Cells were incubated with

TRITC-conjugated phalloidin, anti-osteopontin, its secondary antibody (Millipore Cat. no. AP124F), and 4, 6-diamidino-2-phrnykinodole (DAPI;Millipore, Billerica,MA, USA) for

1 h to stain actin filaments, focal contracts, and nuclei, respectively. The presence of mineralized nodules (calcium deposition) was determined by staining with ARs and VKs. The ethanol-fixed cells and matrix were stained for 30 min with 40mM alizarinred-S(pH 4.2) and rinsed with water 3 times. After photography, the bound stain was eluted with 10% (wt/vol) cetylpyridinium chloride, and alizarin red-S in samples was quantified by measuring absorbance at 560nm (Victor 3, Perkin Elmer, USA). For VKs, the samples were fixed by ice ethanol, and incubated in 5% sliver nitrate solution (Sigma-Aldrich, Milwaukee, WI, USA) for 30 min with exposure to untraviolet light. Then, samples were rinsed in several changes of distilled water. and incubate slide in sodium thiosulfate solution (5%) for 2-3 minutes. Finally, the samples were rinse for 2 minutes in running tap water followed by 2 changes of distilled water.

3.1.6. Neurogenic Differentiation

HABMSCs were placed at a density of 1.0×10^4 cells/cm^2 and cultured for 1 weeks in Mesenchymal Stem Cell Neurogenic Differentiation Medium (C-28015, PromoCell, Germany). ICC was conducted on week 2 to exhibit the expression of Tuj-1 and NeuN. The

cultured cells were washed in phosphate buffered saline (PBS, Sigma-Aldrich, Milwaukee, WI, USA), fixed in a 4% paraformaldehyde solution (Sigma-Aldrich, Milwaukee, WI, USA) for 20 min, and permeabilized with 0.2% Triton X-100 (Sigma-Aldrich, WI, Milwaukee, USA) for 15min. Cells were incubated with TRITC-conjugated phalloidin, anti-osteopontin, its secondary antibody (Millipore Cat. no. AP124F), and 4, 6-diamidino-2-phrnykinodole (DAPI;Millipore, Billerica,MA, USA) for 1 h to stain actin filaments, focal contracts, and nuclei, respectively. RT-PCR was conducted on week 2. Total RNA was isolated with Trizol reagent (Invitrogen, USA) and used to synthesize cDNA using a first-strand cDNA synthesis kit (Invitrogen, USA) according to the instructions of the manufacturer. The primer information is listed in Table 2. The products were separated by electrophoresis on a 1 % agarose gel and visualized by ultraviolet induced fluorescence.

3.1.7. DNA Microarray analysis

All samples were cultured with proliferation media for 1 week. Total RNA was isolated from confluent cultures of all samples using RNeasy Mini Kit (Qiagen, Chatsworth, CA). DNA microarray analysis was carried out by KURABO Gene-Chip Custom Analysis Service with

Human Genome U133 Plus 2.0 chips containing 38 500 genes/47 000 transcripts variants/54 000 probes (Affymetrix. Inc., Santa Clara, CA). The raw data (Microarray Suite version 5.0, SF = 1; Affymetrix Inc.) were standardized by the global median normalization method using GeneSpring (Silicon Genetics, Redwood City, CA). Normalization was limited by flag values, and the median was calculated using genes that exceeded the Present or Marginal flag restriction. Gene filtering on normalized intensity followed by fold changes (more than twofold) was used to generate the list of genes for expression profiles before or after differentiation. The raw data were deposited in the GEO (GSE9451).

3.2. Results

3.2.1. Characterization of RGO Substrates

Foremost, the characterization of RGO substrates were analyzed. The characteristics of RGO were compared with graphene oxide (GO). XPS study exhibited the RGO used in this study is composed of high ratio of C-C bonds. (Fig. 3.1A) In the XRD result, RGO exhibited the characteristic peak of graphene, around 24°. (Fig. 3.1B) Raman spectroscopy result exhibited that G/D ratio of RGO is higher than that of GO. (Fig. 3.1C) Base on the results, it is confirmed that the RGO have higher sp^2-hybridized C-C bonds than GO, indicating that the RGO used in this study is of fair quality. The magnetic property of RGO was evaluated using physical property measurement system. (Fig. 3.1D) RGO performed magnetic moment well when magnetic field was irradiated while GO performed negative magnetic moment. Maximum magnetic moment of RGO is 1.39×10^{-5} EMU. Then, the qualified RGO were adsorbed on glass substrates to make RGO substrates. The fabricated RGO substrates were observed by optical microscope and scanning electron microscopy (SEM). By morphological studies, we exhibited that RGO was successfully adsorbed on the Glass substrates. (Fig. 3.1E)

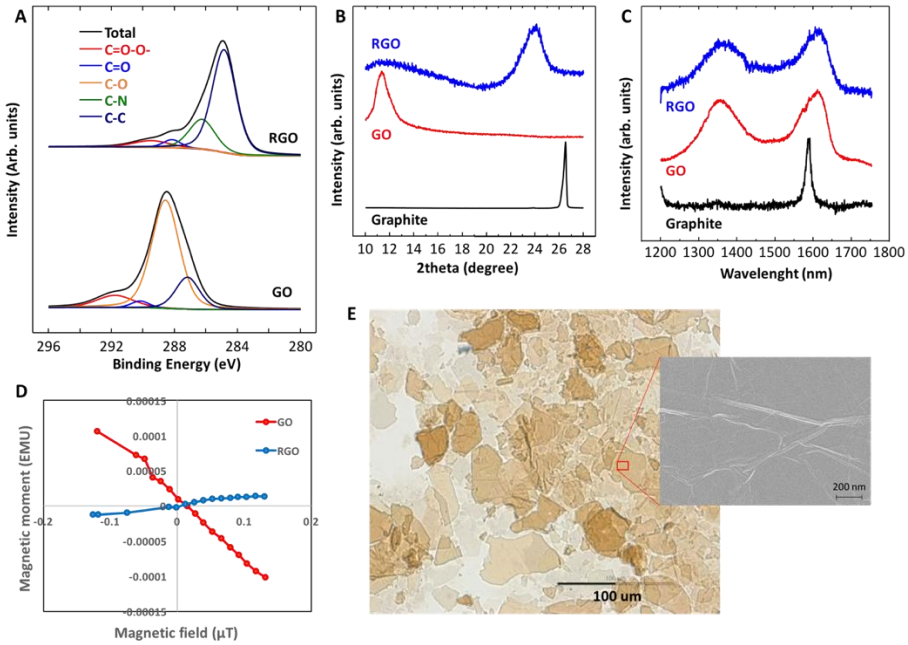

Figure 3.1. Characteristics of RGO and RGO substrates. (A) XPS result. It was confirmed that the RGO is mainly composed of C-C bonds. (B) XRD result. RGO exhibited specific peaks around 25°. (C) Raman spectroscopy result. RGO and GO exhibited D peak and G peak. The G/D peak ratio of RGO was higher than that of GO, indicating that RGO have higher sp^2-hybridized C-C bonds than GO. (D) Magnetometry result of RGO and GO. RGO positively induced magnetic moment that can become electric currents while GO negatively induced magnetic moments. (E) Surface morphology of RGO substrates. Inset: FESEM images of RGO substrates. It was exhibited that RGO was successfully adsorbed on glass substrates.

That was also evaluated by atomic force microscopy (AFM). As a result, RGO substrates exhibited higher roughness. (Fig. 3.2A) Electrical properties of the RGO substrates was measured by cyclic voltametry. (Fig. 3.2B) Its resistance was 661.8 kΩ whereas the resistance of GO was 62.5 gΩ.

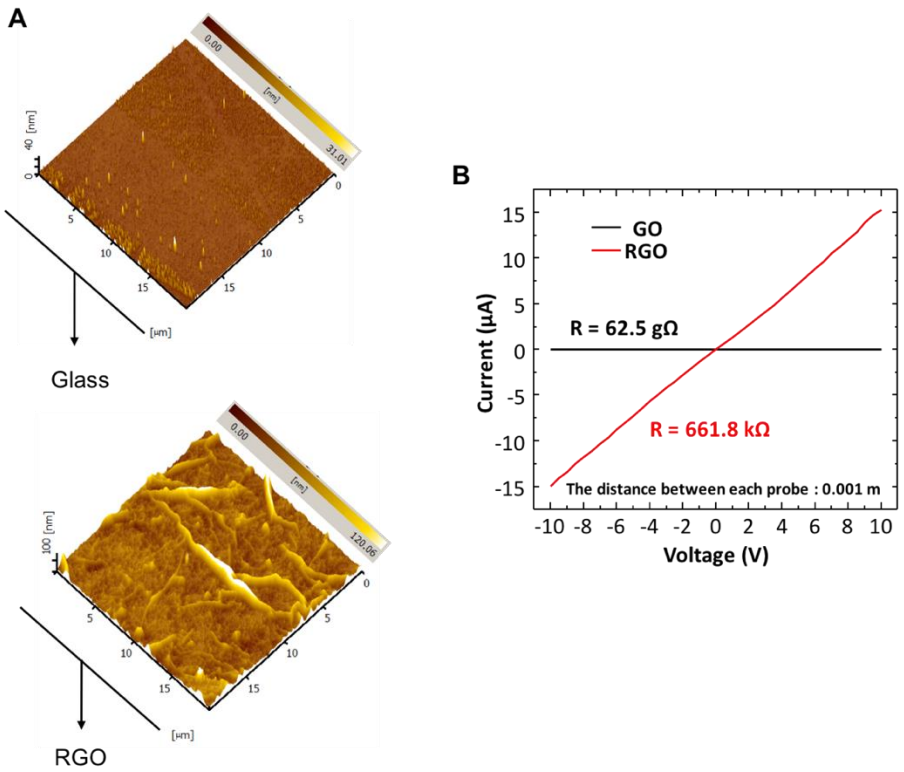

Figure 3.2. Characteristics of RGO substrates.(A) AFM results of Glass and RGO. RGO exhibited rough surface compared to Glass. (B) cyclic voltametry result of RGO substrate. It was compared with GO substrate.

Based on the results, the resistance of RGO substrate was 661.8 kΩ while that of GO substrate was 62.5 gΩ.

3.2.2. Application of PEMFs on RGO Substrates

After characterization of RGO substrates, an *in vitro* study was assessed. The characterisitics of hABMSCs were preferentially investigated using fluorecence-activated cell sorter (FACS). In this results, the hABMSCs highly expressed MSCs marker, e.g., CD13 (97.3 ± 0.4%), CD90 (99.9 ± 0.1%), and CD146 (97.3 ± 0.2%) while CD34, the marker of hemopoietic stem cells, were poorly expressed (5.6 ± 0.2%). (Fig. 3.3) Based on the results, hABMSCs used in this study was confirmed as MSCs with very high purity.

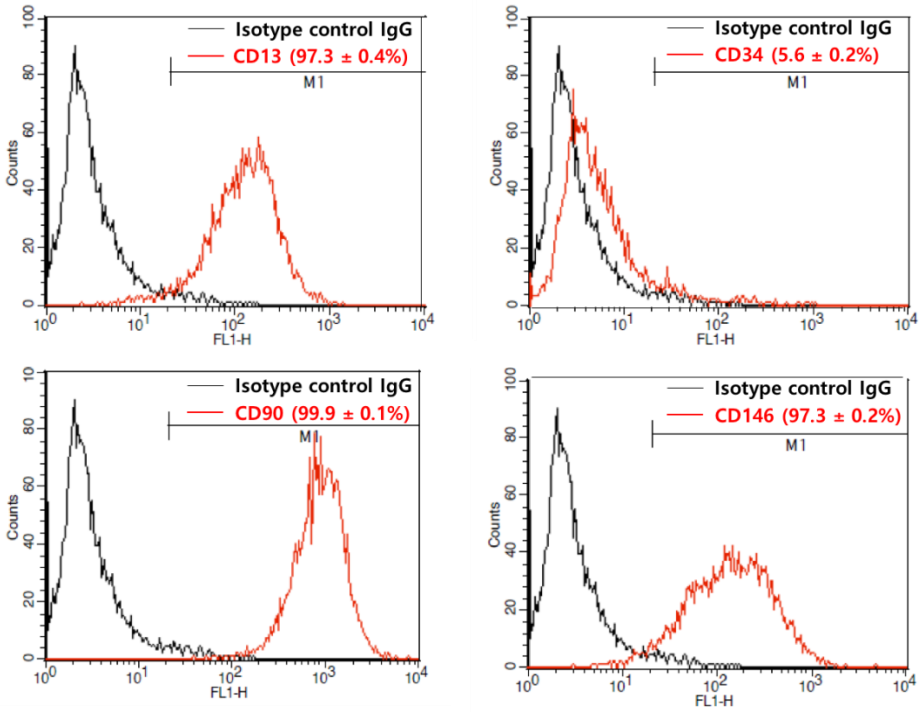

Figure 3.3. Flow cytometric results of hABMSCs. HABMSCs highly expressed CD13, CD90, and CD146, the surface markers of MSCs. In contrast, hABMSCs poorly expressed CD34, the marker of hemopoietic stem cells.

For an *in vitro* study, four groups were chosen: 1) Glass, the group cultured on glass substrates as control; 2) Glass+PEMFs, the group cultured on glass substrates and irradiated by PEMFs; 3) RGO, the group cultured on RGO substrates; 4) RGO+PEMFs, the group cultured on RGO substrates and irradiated by PEMFs. The PEMFs were irradiated using a solenoid, (Fig. 3.2A) following our previous study. Electric signals, of which condition was square wave, ±5 V, 50 Hz-frequency, and 50%-duty cycle, were generated using a function generator. The condition of resultant PEMFs was 0.6 ± 0.05 mT with 50 Hz and expose time on samples was 30 min/day. At first, their cell viability was compared. Seven days later, as seen in Fig. 3.4D, cells on RGO+PEMFs seemed more than other groups. To quantify, we conducted cell viability test and DNA quantification test. In the cell viability test and gene quantification test, all experimental groups have significantly higher cell viability than control. (Figs. 3.4B and C) RGO+PEMFs showed the highest DNA concentration ratio, which have high significance. ICC was conducted to evaluate the trend of specific protein related with cell viability and differentiation. (Figs. 3.4E and F) Cells were cultured for 7 days and vinculin, related with focal adhesion, and fibronectin, related with extracellular matrix (ECM), were stained and observed. The results

exhibited that vinculin was highly expressed on RGO and RGO+PEMFs. (Fig. 3.4E) Fibronectin were also highly expressed on RGO and RGO+PEMFs. (Fig. 3.4F)

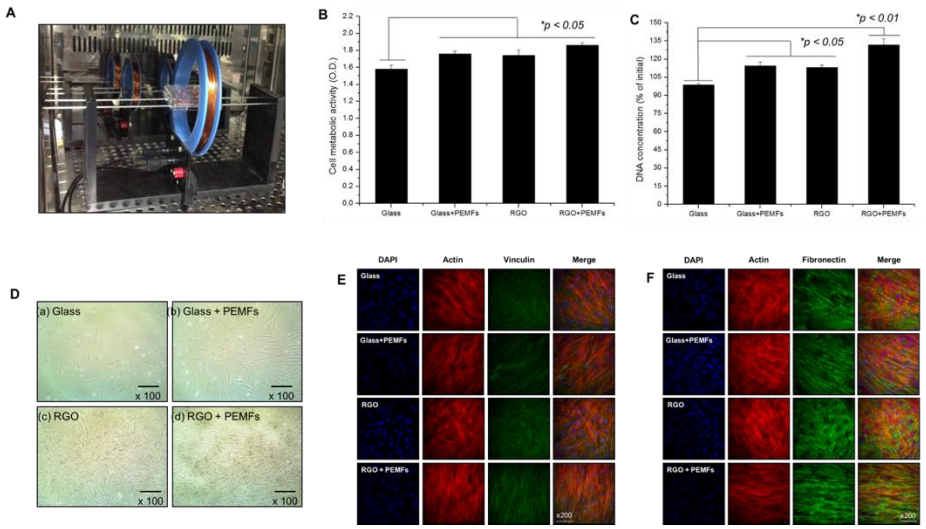

Figure 3.4. Cell viability results by RGO and PEMFs. (A) PEMFs were exerted by a solenoid. By (B) WST and DNA (C) quantification results, all experimentral groups recorded higher cell viability than Glass. RGO+PEMFs exhibited the highest cell viabiltiy. (D) By microscopy images, all experimental groups deemed higher cell number than Glass. HABMSCs looked the highest cell number, supporting the cell viabiltiy results. ICC result of (E) vinculin and (F) fibronectin exhibited that not only RGO and PEMFs enhanced their expressions. RGO+PEMFs are expected to synergically enhance their expressions.

3.2.3. Differentiation Study

The synergic effects by RGO substrates and PEMFs were examined on the osteogenesis of hABMSCs. (Fig. 3.5) All groups were cultured using osteogenic media and investigated on week 1 and 2. ALP activity was measured on week 1 and ICC, RT-PCR, ARs, and VKs were conducted on week 2. ALP activity study showed that ALP was highly secreted on RGO+PEMFs on week 1. (Fig. 3.3B) ICC result exhibited that osteopontin (OPN), the late osteogenic marker, was expressed highest on RGO+PEMFs on week 2. (Fig. 3.5A) RT-PCR results exhibited that genes related with osteogenic differentiation - RUNX-2, OPN, OCN, BSP, and SMAD-1 - are better expressed on RGO+PEMFs than those on Glass. (Fig. 3.5C) Inversely, gene expression of ALP decreased, indicating RGO+PEMFs turned to late osteogenic stage faster than Glass. Mineralization by RGO or PEMFs was assessed. According to ARs and VKs results, RGO+PEMFs exhibited the highest mineralization. (Figs. 3.5D and E)

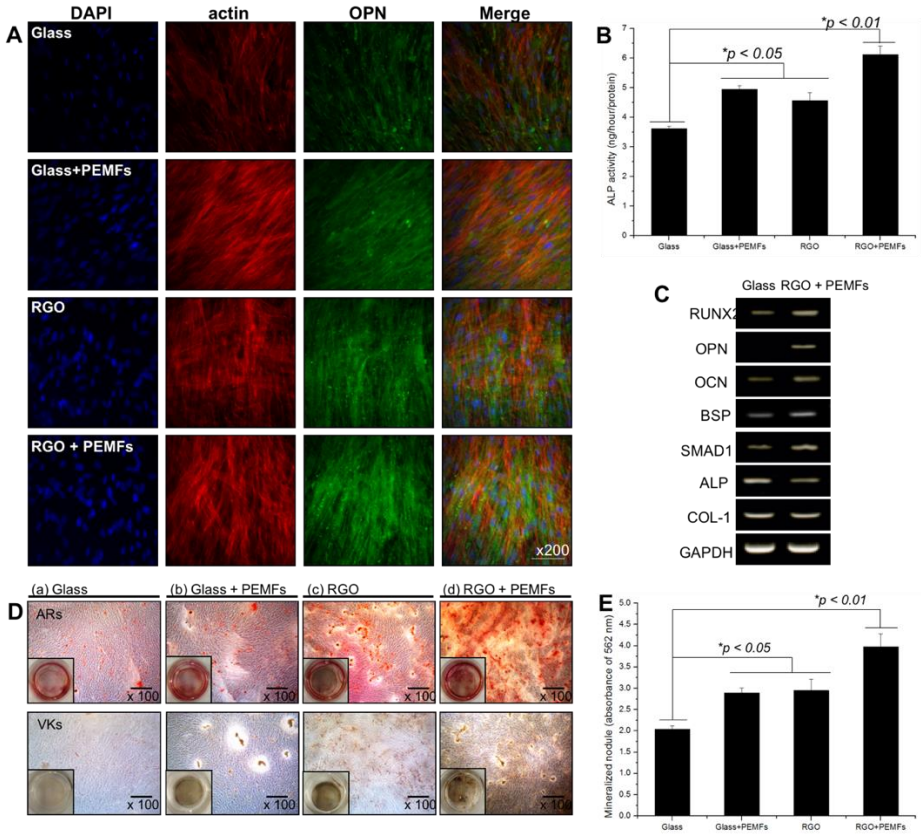

Figure 3.5. Osteogenic differentiation by RGO and PEMFs. (A) ICC results staining OPN. It indicated that OPN is expressed the best on RGO+PEMFs. (B) ALP activity result on week 1. The RGO+PEMFs exhibited the highest activity. (C) RT-PCR result of Glass and RGO+PEMFs. RGO+PEMFs enhanced the expressions of RUNX2, OPN, OCN, and BSP - the significant indicators of osteogenic differentiation. (D) ARs and VKs results by RGO and PEMFs. RGO+PEMFs exhibited the strongest staining. It was quantitatively proved by (E) the destaining of ARs.

Besides, neurogenic capability of RGO+PEMFs was studied. (Fig. 3.6) The Glass and RGO+PEMFs were cultured with neurogenic media for 7 days and their characteristics were assessed by ICC and RT-PCR. According to Fig. 3.6A, Tuj-1, the early marker of neurogenic differentiation, were well expressed on all groups. By the way, NeuN, the late marker of neurogenic differentiation, were better expressed on RGO+PEMFs. (Fig. 3.6A) According to RT-PCR result, RGO+PEMFs increased nestin and MAP2 expression, the important markers of neurogenic differentiation, compared with Glass. (Fig. 3.6B)

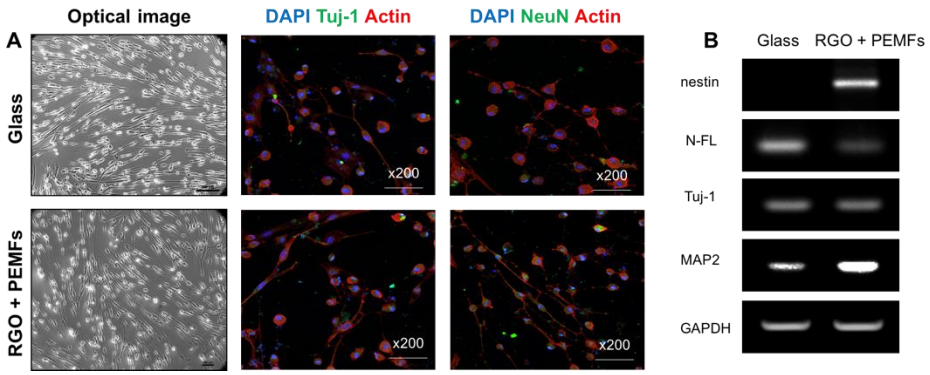

Figure 3.6. Neurogenic differentiation by RGO+PEMFs. (A) Optical images and ICC images of Glass and RGO+PEMFs. The samples equivalantly changed the morphology of hABMSCs and expression of Tuj-1. Interestingly, RGO+PEMFs enhanced the expression of NeuN, the later marker of neurogenesis. (B) RT-PCR results by Glass and RGO+PEMFs. RGO+PEMFs promoted the expression of nestin and MAP2, the important markers of neurogenic differentiation.

Moreover, the chondrogenic and adipogenic capability of RGO+PEMFs were investigated. (Fig. 3.7) Glass and RGO+PEMFs were cultured for 7 days using chondrogenic and adipogenic media. According to RT-PCR result, gene expressions of ALBP, AP-9, and LPL were increased, indicating that RGO+PEMFs increased adipogenesis. However, the gene expression of Sox9, ACAN, and COL II of RGO+PEMFs were downregulated. Thus, RGO+PEMFs decreased chondrogenesis of hABMSCs.

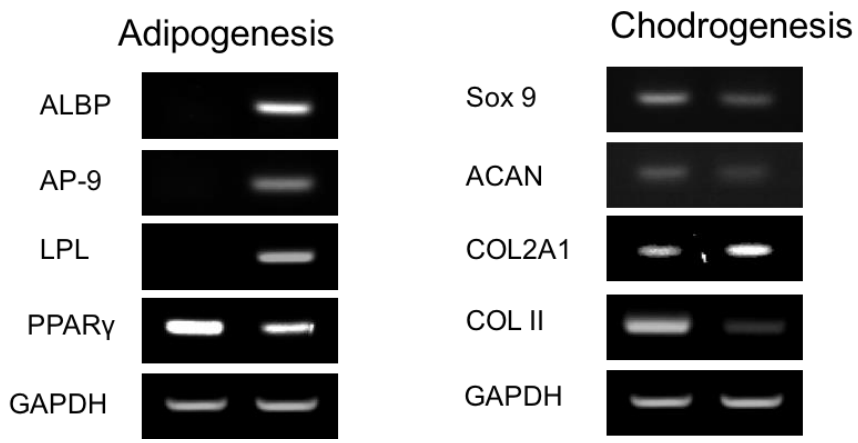

Figure 3.7. RT-PCR results of hABMSCs under adipogenic and chondrogenic differentiation. RGO+PEMFS enhanced the expression of ALBP, AP-9, and LPL, the markers of adipogenesis. However, RGO+PEMFs decreased the expression of Sox 9, ACAN, and COL Ⅱ, the markers of chondrogenesis.

3.2.4. DNA Microarray

DNA microarray study was investigated to verify the brief mechanisms of RGO and PEMFs on hABMSCs differentiation. (Fig. 3.8) In this study, 34,127 probes were analyzed on each sample. (n=3) The genes of Glass+PEMFs, RGO, and RGO+PEMFs were compared with Glass Together, genes of RGO+PEMFs were compared with RGO. In the results of RGO vs. Glass, 137 genes exhibited significant differences.

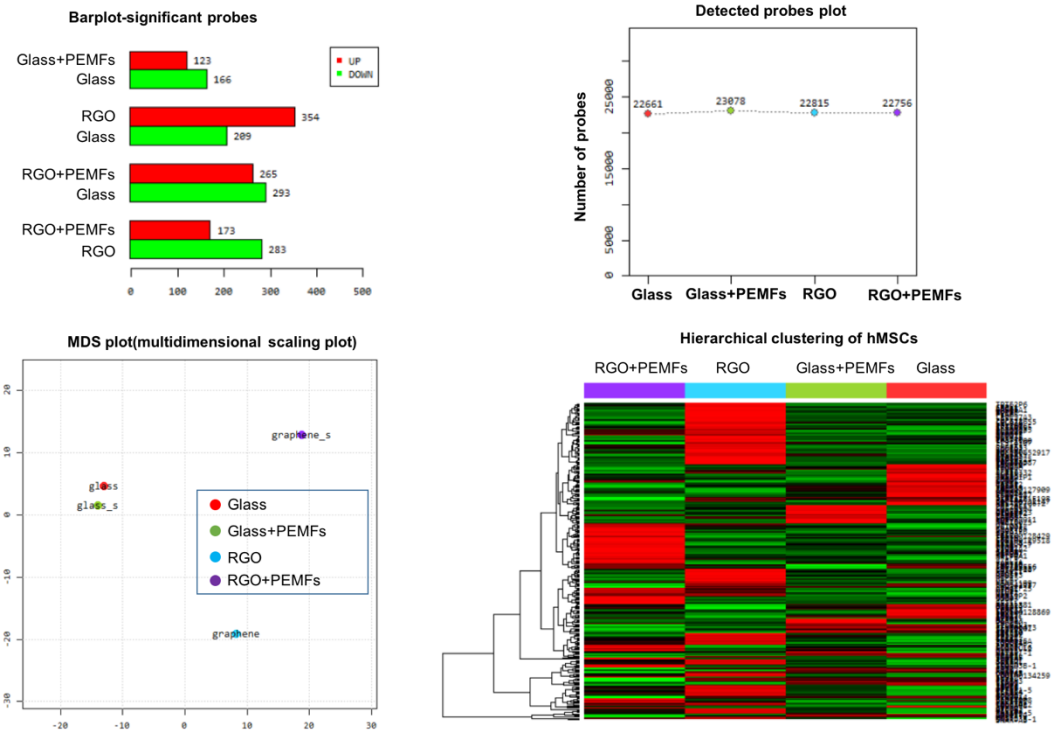

Figure 3.8. DNA microarray result. In this study, 34,127 probes were analyzed on each sample.

By database for annotation, visualization and integrated discovery (DAVID) analysis, the genes clustered by ECM, metabolism, hormone, homeostasis, and osteogenesis exhibited significant differences (Fig. 3.9A). In Glass+PEMFs vs. Glass result, 56 genes exhibited significant differences. DAVID analysis showed that genes related with ion transport and transcription exhibited significant differences (Fig. 3.9B) In RGO+PEMFs vs. Glass result, 122 genes exhibited significant differences. DAVID result exhibited that the genes related with Ca^{2+} signaling and cell-cell communication were significantly different. (Fig. 3.9C) In RGO+PEMFs vs. RGO, 109 genes exhibited significant differences. DAVID result exhibited that the genes related with ECM and plasma membrane were significantly different. (Fig. 3.9D) Not only clustered groups, some representative genes were also compared. In Fig. 3.9E, RGO upregulated genes related with differentiation, metabolism, and angiogenesis while downregulated genes related with volate-gated channels compared to Glass. Particularly, calbidin 2 (CALB2) and stanniocalcin 1 (STC1), related with neurogenic differentiation, were significantly increased although neurogenesis wasn't detected in DAVID analysis. Inhibin beta B (INHBB) and solute carrier family 2 member 5 (SLC2A5), related with adipogenic differentiation, were also

significantly increased. Further, gene expressions of RGO+PEMFs were compared with RGO. (Fig. 3.9F) As a result, RGO+PEMFs enhanced the genes related with Ca^{2+} signaling, proliferation, and neurogenesis. Especially, jagged 2 (JAG2), related with notch signaling and Ca^{2+} signaling, were almost 100 times increased. To evaluate the influence of RGO and PEMFs on Ca^{2+} signaling, ICC which stained calmodulin (CaM), the regulator of Ca^{2+} signaling, was conducted. As a result, it was observed that CaM expression on Glass+PEMFs and RGO+PEMFs was better than those of Glass and RGO. (Fig. 3.9G)

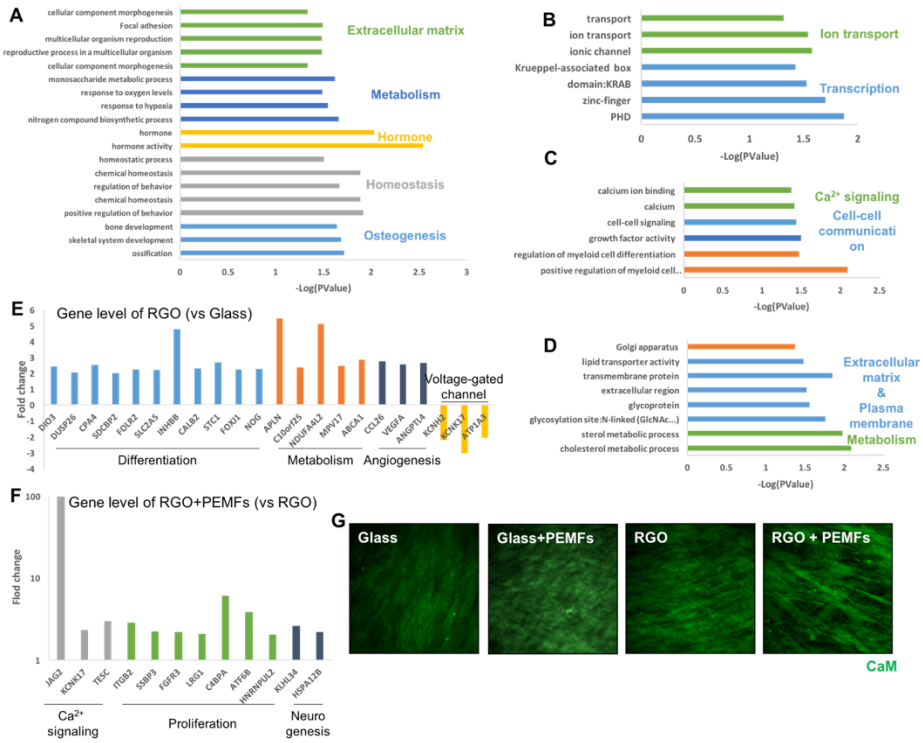

Figure 3.9. DNA microarray results. (A) DAVID result of RGO compared with Glass. The genes related with ECM, metabolism, hormone, homeostasis, and osteogenesis exhibited significant differences. (B) DAVID result of Glass+PEMFs compared with Glass. The genes related with ion transport and transcription were significantly different. (C) DAVID result of RGO+PEMFs compared with Glass. RGO+PEMFs induced significant differences of the genes related with Ca^{2+} signaling and cell-cell communication. (D) DAVID result of RGO+PEMFs compared with RGO. RGO+PEMFs induced significant differences of the genes related with golgi apparatus, ECM, cell membrane, and metabolism. (E) Representative genes of RGO exhibiting significant differences compared with Glass. RGO upregulated genes related with differentiation, metabolism, and angiogenesis while downregulated genes related with volate-gated channels compared to Glass. (F) Representative genes of RGO+PEMFs exhibiting significant differneces compared with RGO. RGO+PEMFs enhanced the genes related with Ca^{2+} signaling, proliferation, and neurogenesis. (G) ICC results of CaM. In case of Glass+PEMFs and RGO+PEMFs, CaM expression is increased, indicating that PEMFs enhanced ca^{2+} signaling.

3.4. Discussion

Stem cells are undifferentiated cells that can differentiate into many lineages, such as bone, muscle, cardiomyocyte, fat, neuron, etc. [102] Because of its self-renewal and differentiation capability, cell and tissue engineering field paid lots of attention to stem cells. Many researchers devoted to efficient differentiation of stem cells into the specific somatic cells for relevant regeneration. One of easy way to differentiate stem cells is to induce chemical components. The fate of stem cells is modulated by the variety of chemical components. For example, dexamethasone, β-glycerophosphate, and ascorbic acid promote osteogenic differentiation. [49] Insulin-transferrin-selenium, basic fibroblast growth factor, and retinoic acid promote neurogenic differentiation. [103] Further, insulin and isobutylmethylxanthine are known to promote adipogenic differentiation. [104] Addition of nanomaterials such as gold and silver nanoparticles were reported to promote the differentiation of stem cells, too. [105-106] Carbon-based nanomaterials were also reported to promote osteogenic differentiation of MSCs. [107] Among them, graphene is recently reported nanomaterials to promote osteogenic differentiation of MSCs [108] as well as neurogenesis. [65] Recently the functionality of graphene is getting a

spotlight on the cell and tissue engineering fields. Electrical stimulation-combined graphene was synergically effective on osteogenesis and neurogenesis. [68-69] Especially, EMFs inducing with electroconductive nanoparticles are expected to have synergic effects. However, the application of EMFs and electroconductive nanoparticles simultaneously have never been tried yet. In this study, in our knowledge, RGO and EMFs was applied on the differentiation of MSCs for the first time.

Figures 3.1A-C represents the chemical properties of RGO. By the XPS result, it was confirmed that the RGO is mainly composed of C-C bonds. Moreover, in the raman spectroscopy result, D peak is comprised due to sp^2-hybridized C-C bonds and G peak is comprised due to sp^3 C-C bonds. Because G/D peak ratio of RGO was higher than that of GO, it is confirmed that the C-C bond in the RGO mainly consist of sp^2-hybridized C-C bonds. The magnetometry of the RGO was also measured. The RGO was positively reacted with magnetic field whereas the GO was negatively reacted with the magnetic field. It indicates that magnetic field-irradiated RGO can induce magnetic moments, which causes induced electric currents when magnetic fields are changed. The maximum magnetic moment induced on RGO was 1.39×10^{-5} EMU. If

electric currents ideally invoked, it would be 13.9 × 10 mA/m^2. In the *in vitro* study, Glass+PEMFs, RGO, and RGO+PEMFs increased cell viability. (Fig. 3.3) It was reported that cell adhesion, ECM, and cell viability are deeply correlated. [109] In Figs. 4.3E and F, all experimental groups enhanced expression of vinculin and fibronectin. Based on the microarry results, Glass+PEMFs enhanced ion transport and transcription. Further, RGO enhanced cell adhesion, ECM, and membrane protein. Those indicate that Glass+PEMFs and RGO affected cell viability by indipendaent pathways. It is supposed that the apparent pathways were maximized on RGO+PEMFs. As a result, RGO+PEMFs recorded the highest cell viabiltiy. Consistently, expressions of vinculin and fibronectin were highest on RGO+PEMFs According to microarray results, RGO+PEMFs enhanced cell-cell communication, metabolism, and proliferation. (Fig. 3.9C) Further, RGO+PEMFs synergically enhanced ECM, and cell membrane. (Fig. 3.9D) Consequently, it is expected that RGO and PEMFs synergically enhanced the cell viability, cell adhesion, and ECM formation.

In the differentiation study, RGO+PEMFs enhanced osteogenic differentiation. RGO+PEMFs promoted early expression of ALP, early marker of osteogenesis, on week 1. (Fig. 3.6B) On week 2,

RGO+PEMFs promoted OPN as well as RUNX2, OCN, BSP, and SMAD1 expression. (Figs. 3.6A and C) RGO+PEMFs also promoted calcium deposition rate. (Figs. 3.6D and E) RGO+PEMFs also enhanced neurogenesis. ICC and RT-PCR results exhibited that RGO+PEMFs upregulated nestin and MAP2. (Fig. 3.7) Further, RGO+PEMFs promoted adipogenesis. (Fig. 3.8) Actually, PEMFs were reported to promote osteogenic differentiation. [49] The main reason is that PEMFs promote the Ca^{2+} efflux and it would results in the upregulation of many signaling pathways including ERK and wnt which are very important signaling pathways related with osteogenic differentiation. [45] In this study, PEMFs promoted ion transport as well as ca^{2+} signaling. (Figs. 3.9B and D) Moreover, CaM, a regulator of calcium transport, upregulated on Glass+PEMFs and RGO+PEMFs. Consequently, it is confirmed that PEMFs promoted ca^{2+} signaling, resulting in the promotion of osteogenic differentiation. Moreover, it is meaningful that this study devoted to reveal the mechanism of graphene on the differentiation of stem cells. Up to date, the biological effects of graphene were reported several times. However, the mechanism of graphene on promoting stem cell differentiation has not been reported well. In this study, the mechanism why graphene promotes stem cell

differentiation was reported by microarray. (Fig. 3.9A) The RGO promoted the proteins related with differentiation, e.g., DIO3, DUSP26, and CPA4. (Fig. 3.9E) It promoted proteins related with osteogenic differentiation, SDCBP2 and FOLR2. Together, RGO promoted STC1 and CALB2, related with neurogenesis. RGO also promoted CCL26 and INHBB, related with adipogenesis. Moreover, RGO promoted metabolism and angiogenesis, deeply related with osteogenic differentiation. [110] For separating the synergic effects by RGO+PEMFs, the microarray results of RGO and RGO+PEMFs were compared. RGO+PEMFs upregulated Ca^{2+} signaling and cell-cell communication. (Fig. 3.9C) Compared with RGO, RGO+PEMFs enhanced ECM, membrane protein, proliferation and metabolism. (Figs. 3.9D and E) Moreover, KLHL34 and HSPA12B, related with neurogenesis, were upregulated stronger than those of RGO. (Fig. 3.9E) Compared to Glass+PEMFs, RGO+PEMFs significantly upregulated signaling pathways related with ECM, membrane protein, and metabolism. These seemed to be deeply related with the microelectric current on RGO invoked by PEMFs. Electric stimulation on MSCs were reported to promote ECM, membrane protein, and metabolism. [111] Consequently, RGO+PEMFs promote the differentiation of hABMSCs not only by

RGO and PEMFs, but also by synergic effect - microelectric current invoked by PEMFs. (Fig. 3.10)

This system is anticipated to overcome the limitation of RGO-based platforms. RGO is a kind of graphene family, made by reducing GO. Its purity cannot overcome the graphene fabricated by chemical vapor deposition method. Further, the electric resistance of RGO substrates is much higher than that of CVD graphene because RGO are disconnected each other, resulting in high resistance. Thus, these days the RGO-based systems are not prefered as platforms inducing mechanical stimulations in tissue engineering. By the way, we invoked electric current by PEMFs. Because induced electric current can be generated on local area, the substrate doesn't have to be connected each other, that is, this systems can overcome disconnection problem. Another advantage of this system is that this system can be applied in the traditional tissue engineered scaffolds. By incorporating RGO, this system can be easily combined with them. It was known that RGO is hard to apply in tissue engineering because it is not well dispersed in organic or inorganic solvent. However, RGO can be dispersed well if the size of RGO is small enough. Moreover, it can be applicable in clinical study as well as *in vivo* study by combining with biodegradable scaffolds.

Particularly, EMFs can be exerted on the transplanted scaffolds noninvasively. Thus, this system can be easily applied in clinical study as well as *in vivo* study. Other stimulation systems, electrical, light, etc., have limitations to be applied in *in vivo* study. On the other hand, EMFs stimulation is already commercialized in clinical application. Thus, it is expected that EMFs stimulation system would come true in tissue engineering-based therapy. That would become a turning point in tissue engineering and regenerative medicine.

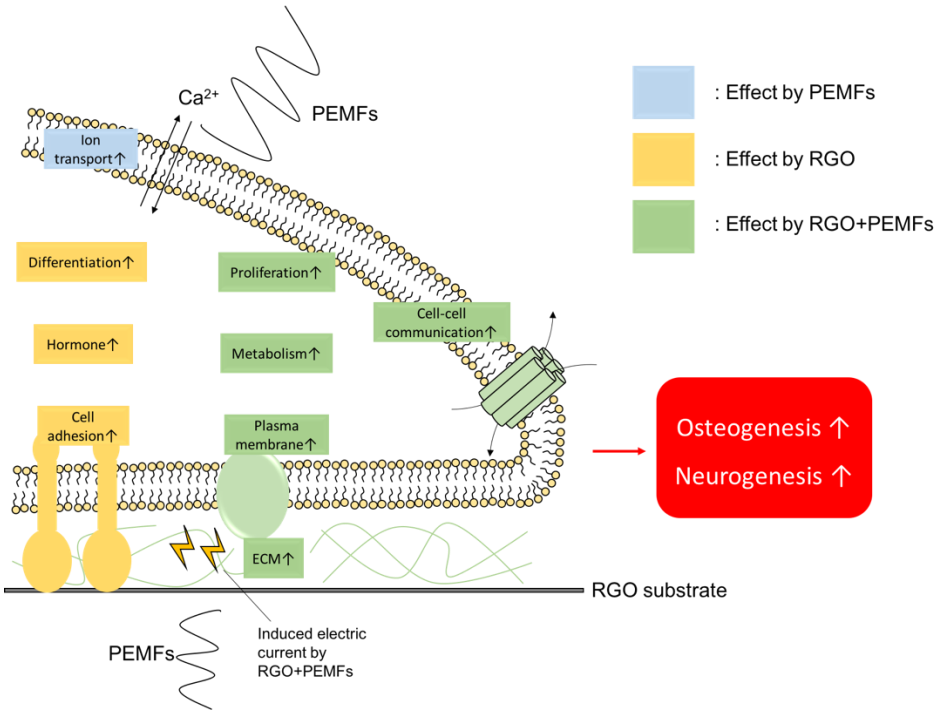

Figure 3.10. Brief mechanism of RGO and PEMFs on hABMSCs. PEMFs enhanced the ion transport and transcription. On the other

hand, RGO enhanced cell adhesion, hormone secretion, and differentiation capacity. When RGO and PEMFs exerted on hABMSCs simultaneously, they synergically enhanced ECM formation, cell membrane protein, metabolism, proliferation, and cell-cell communication. This synergic effects is due to electric current induced on RGO by PEMFs. ECM formation, cell membrane, metabolism, and cell-cell communiciation is deeply related with the differentiation of stem cells. Consequently, the application of RGO and PEMFs at the same time would promote the differentiation of MSCs, particulary for osteogenesis and neurogenesis.

4. Part Ⅱ: Graphene-reinforced nanocomposite bone cements for bone tissue engineering

4.1. Materials and Methods

4.1.1. Preparation of RGO-incorporated micro/nano-sized natural bone powder mixture

The preparation method for micro/nano-sized natural bone powders followed the preliminary study. [28] Briefly, horse bones (Jejushopping, Republic of Korea) were soaked in distilled water to drain the remaining blood for 24 hours. Then, the bones were immersed in hydrogen peroxide (Duksan Chemicals Co, Korea) for 72 hours. After soaking, the flesh on surface was cut out, and the horse bones were sintered in an electric furnace (UP350E, Yokogawa Co, Japan) at 1200 ℃ for 2 hours. The sintered bones were ground into powders using a miller (A10, IKA-WERKE, Japan) and the ground bone powders were sintered three more times. Micro-sized horse bone powders of which the particle size was below 100 μm were collected by sieve (Daihan Scientific, Korea). Nano-sized horse bone powders were ground by a Nano Sizer Fine Mill (Deaga Powder Systems Co. Ltd., Republic of Korea), a device that pulverizes and disperses particles by friction between beads and a

revolving screen. The collected micro/nano-sized powders were mixed 50:50 (w/w) and RGO was incorporated into the powders by 10000:1, 1000:1, and 100:1 (w/w). The resultant concentrations of RGO were 0, 0.01, 0.1, and 1 wt%, respectively.

4.1.2. Fabrication of RGO-CPCs

A 3.5% chitosan (CS) solution for hardening CPCs was prepared by dissolving chitosan (Molecular weight: 200,000, D: 90%, Taehoon Co, Korea) in 2% lactic acid (v/v, #50215, Duksan Chemicals Co, Korea) solution. The prepared powders and CS solution were thoroughly mixed with ratios of 0.45:1 (v:w) and placed into a polydimethylsiloxane (PDMS) mold (6 φ diameter, 2 mm height) at 37 ℃ and 100% humidity for 4 hours. The fabricated RGO-CPCs were classified following the RGO concentration in powders. Detailed information is listed in Table 3.1.

Table 3.1. Nomenclature of experimental group

Abbreviation	Bone powder	RGO (%, w/w)	3.5% CS sol. (w/v)
No RGO	O	-	0.45
0.01% RGO	O	0.01	0.45
0.1% RGO	O	0.1	0.45
1% RGO	O	1	0.45

4.1.3. Morphological analysis

The fabricated CPCs were dried completely at room temperature, and observed by a field emission scanning electron microscope (FESEM, SUPRA 55VP, Carl Zeiss, Germany). The points of study were determined and analyzed with energy-dispersive X-ray spectroscopy (EDS) EDS mounted in FESEM (SUPRA 55VP, Carl Zeiss, Germany). This resulted in a histogram, where the horizontal axis displays units of energy [kilo electron volts (keV)] and the vertical axis represent the intensity.

4.1.4. Chemical properties analysis

The presence of crystalline phases on the RGO-CPCs according to bone powder and RGO was detected by x-ray diffraction (XRD) and Raman spectroscopy. In XRD, an X-ray diffractometer (New D8 advanced XRD, Bruker, Germany) with copper Kα radiation at 40 kV and 40 mA was used. The samples were scanned from 20 to 65° using steps of 2 theta with a counting time of 60 s per step. The crystalline phase compositions were identified with reference to standard JCPDS cards available in the system software. The Raman spectra of the RGO-CPC was obtained with a T64000 (Horiba Jobin Yvon) at an excitation wavelength of 514.54 nm. X-ray photoemission spectroscopy (XPS) was conducted on a Sigma Probe (ThermoVG, U.K) operating at a base pressure of $5 \times 10 - 10$ mbar at 300 K with a nonmonochromatized Al K α line at 1486.6 eV, a spherical sector analyzer of 180 °, a mean diameter of 275 mm, an analysis area of 15 μm to 400 μm, and multichannel detectors.

4.1.5. Analysis of mechanical properties

The mechanical properties of the RGO-CPCs were analyzed using a texture analyzer (TAXT2i, Stable Microsystems Co, US). The prepared CPCs samples (6 φ diameter, 2 mm height) were compressed at a crosshead speed of 1 mm/min until failure, and the stress-strain diagram of the samples were recorded. From the diagrams, the elastic modulus, maximum allowable strain, and maximum compressive stress were calculated.

4.1.6. Soaking test

To perform the bioactivity test, simulated body fluid (SBF) was prepared by dissolving NaCl, $NaHCO_3$, KCl, $K_2HPO_4 \cdot 3H2O$, $MgCl_2 \cdot 6H2O$, and Na_2SO_4 in distilled water and HCl to reach a pH value of 7.4, following the protocol of Kokubo et al. [30] Each bone cement specimen was immersed in 500 μl of SBF for 7, 14, or 21 days at 37℃ and 100% humidity. The SBF was replaced with fresh SBF every week. After the due date, each specimen was collected and dried at 37℃ and 100% humidity. The dried samples were weighed, and their mechanical properties were analyzed by texture analyzer.

4.1.7. *In vitro* study

4.1.7.1. Cell culture

A mouse calvaria-derived osteoblast cell line, MC3T3-E1 (CRL-2593, ATCC, USA) was cultured in proliferation media. The proliferation medium was α-MEM (#LM 008-02, WELGENE Inc., Korea) supplemented with 10% fetal bovine serum (FBS, #SH30919.03, Hyclone, USA), 1% antibiotics (#LS 203-01, WELGENE Inc., Korea) at 37℃ in 5% CO_2 conditions. The media was changed every other day.

To isolate rASCs, subcutaneous fat tissues (2 ml volume) in the operation site were obtained from a rat. Tissues were washed with phosphate buffered saline (PBS; Gibco, Milan, Italy), digested with 100 U/mL collagenase type I (Sigma-Aldrich, St. Louis, MO) in low glucose Dulbecco's modified Eagle's medium (DMEM; Gibco-BRL, Grand Island, NY), and incubated for 8 hours to lyse the adipose tissues. The stromal fraction was collected by centrifugation and then passed through a cell strainer (100 ml size) to remove any large cell clumps and particles. For the cell culture and expansion of adipose-derived cells, cells were grown in low glucose DMEM with 10% fetal bovine serum (FBS; Gibco, Milan, Italy) and 1% penicillin–streptomycin (Gibco, Milan, Italy) at 37℃ in a 5% CO_2 atmosphere. To confirm the phenotypic characterization of the rASCs, undifferentiated cells were cultured in stromal DMEM media. If the cells were more than 80% confluent, the cells were harvested using trypsin–EDTA and resuspended at a concentration of 1×10^6 cells/ml in fluorescence activated cell sorting (FACS) buffer. Cells were firstly stained using fluorescein isothiocyanate (FITC)-conjugated antibody CD105 (mesenchymal stem cell marker) for 1 h at 4℃ and FACS was performed using FACS DiVa software (BD Bio- sciences, San Jose, CA).

4.1.7.2. Cytotoxicity test

A concentration of 1×10^4 cells/well MC3T3-E1 and rASCs were seeded on 96-well plate and incubated at 37℃ in a 5% CO_2 atmosphere for 1 day. RGO-CPCs were put into another 96-well plate. They were immersed in 200 μl culture media and incubated at 37°C in a 5% CO_2 atmosphere for 24 h. After soaking, the culture media were collected. Then, cell-cultured media were removed and the collected culture media from the RGO-CPCs were added to the plate and incubated for 12 and 24 h. Following the incubation, the cytotoxicity was measured by WST-1 (EZ-Cytox Cell Viability Assay Kit, EZ3000 Daeillab Service Co., Seoul, Republic of Korea).

4.1.7.3. Adhesion test

Each RGO-CPC was added to a 96-well plate. 1×10^4 cells/well MC3T3-E1 and rASCs were seeded on RGO-CPCs and incubated at 37℃ in a 5% CO_2 atmosphere for 6 h. Following the incubation, media were removed and PBS were added to the wells to gently wash out unattached cells. After washing, fresh media were added to the wells and

the cell adhesion was measured by WST-1 (EZ-Cytox Cell Viability Assay Kit, EZ3000 Daeillab Service Co., Seoul, Republic of Korea).

For immunocytochemistry (ICC), MC3T3-E1 and rASCs (1×10^4 cells/sample) were seeded onto RGO-CPCs, and allowed to spread for 1 or 7 days in culture media at 37℃ in a humidified atmosphere containing 5% CO_2. Adhered cells were fixed with a 4% paraformaldehyde solution (Sigma-Aldrich, Milwaukee, WI) for 20 min, permeabilized with 0.2% Triton X- 100 (Sigma-Aldrich, WI, Milwaukee) for 15 min, and stained with TRITC-conjugated phalloidin (Millipore, Billerica, MA) and 4, 6-diamidino-2-phrnykinodole (DAPI; Millipore, Billerica, MA) for 1 h. Focal adhesions (FAs) were stained with a monoclonal anti-vinculin antibody (1:100; Millipore, Billerica, MA) and an FITC-conjugated goat anti-mouse secondary antibody (1:500; Millipore, Billerica, MA). Images of the stained cells were taken using a confocal laser scanning microscope (LSM710, Carl Zeiss, Germany).

4.1.7.4. Cell viability test

Each RGO-CPC was added to a 96-well plate, and 1×10^4 cells/well MC3T3-E1 and rASCs were seeded on the RGO-CPCs and incubated at 37℃ in a 5% CO_2 atmosphere for 1, 3, or 7 days. Following the incubation, cell viability was measured by WST-1 (EZ-Cytox Cell Viability Assay Kit, EZ3000 Daeillab Service Co., Seoul, Republic of Korea).

4.1.7.5. Cellular morphology analysis

MC3T3-E1 and rASCs adhered and proliferated on RGO-CPCs were observed by FESEM. Briefly, 1×10^4 cells were seeded on the CPCs and incubated for 1 and 7 days at 37℃ in 5% CO_2 conditions. Then, 2 mL of modified karnovsky's fixative solution was filled in the 24 well-plate and stored for 2 hours at 4℃ for primary fixation. The primary fixing solution was then removed, and the cultured bone cement specimens were washed with 0.05 M sodium cacodylate buffer three times at 4℃ for 10 min. The specimens were soaked in 2 mL of 1% osmium tetroxide solution for 2 hours for post fixation. After the solution was removed, the plate was washed two times briefly with distilled water at a room temperature. The specimens were dehydrated in 30, 50, 70, 80,

90, and 100% ethanol at room temperature for 10 min., respectively. After soaking in hexamethyldisilazane (HMDS) for 15 min two times for drying, FE-SEM analysis was carried out with a Zeiss Supra 55VP field-emission scanning electron microscope.

4.1.7.6. Migration assay

The migration effect of RGO-CPCs on MC3T3-E1 was assessed with the CytoSelect™ 24-well Wound Healing Assay. Briefly, 24-well plate was coated by RGO-CPCs. Then, inserts were put in the 24-well plate wells and aligned in a single direction, 500μL of cell suspension containing 0.5×10^{6}cells/mL was added to each well and the well plate was incubated at 37.0℃ overnight. The inserts were then removed from each well, and the wound sites were observed by ICC for 3 days.

4.1.7.7. Western blot

The total cellular protein was extracted by RIPA lysis buffer (62.5 mM Tris-HCL, 2% SDS, 10% glycero, pH 7.5) with added proteinase inhibitor cocktail (Invitrogen, USA). Cell lysates were incubated on ice for 30 min and then centrifuged at 13,000 rpm for 30 min at 4℃. Supernatant (protein lysate) was collected and the protein concentration was determined by a micro bicinchoninic acid (BCA) Protein Assay Kit (Bio-rad, Hercules, Calif). Twenty five μg-aliquots of the cell lysates were separated by 8% SDS-PAGE under reducing conditions. Separated proteins were transferred to a PVDF membrane (Millipore Corporation, Bedford, MA, USA) at 30 V for 1 h. After blocking with 5% skim milk in PBST, the membranes were incubated overnight in primary antibody at 4℃. Then, the primary antibody was removed and washed thrice by PBST for 10 min. each. After washing, samples were incubated with a secondary antibody for 2 h at room temperature. After incubation, the secondary antibody was removed and washed thrice using PBST for 10 min. Anti-alkalinephosphatase (ALP, ab354, Abcam, Cambridge, MA, USA), Runt-related transcription factor-2 (Runx-2, ab23981, Abcam, Cambridge, MA, USA), and osteocalcin (OCN, AB10911, Millipore, USA) were used as the primary antibodies and horse raddish peroxidase

(HRP)-conjugated anti-rabbit immunoglobulin G (G21234, Invitrogen, USA) was used as the secondary antibody. Quantification of the Western blot was performed using the Image J software with a normalization of the level of the entire protein.

4.1.7.8. Alizarin red staining (ARS)

MC3T3-E1 and rASCs were fed with α-MEM and DMEM media to which 50 μg/mL ascorbate-2-phosphate (Sigma-Aldrich, WI, Milwaukee) and 10 μM dexamethasone (Sigma-Aldrich, WI, Milwaukee) were added for 2, 3, and 4 weeks, respectively. Calcium precipitation of the ECM was visualized by staining with ARS (Sigma-Aldrich, WI, Milwaukee). Briefly, the ethanol-fixed cells and matrix were stained for 1 hour with 40 mM ARS (pH 4.2) and extensively rinsed with water. After photography, the bound stain was eluted with 10% (wt/vol) cetylpyridinium chloride, and the ARS in samples was quantified by measuring the absorbance at 544 nm.

4.1.8. *In vivo* study

4.1.8.1. In vivo transplantation of RGO-CPCs with hABMSCs in immunocompromised mice

To evaluate the effects of RGO-CPCs on mineralized tissue formation of mesenchymal stem cells in vivo, human alveolar bone marrow stem cells (hABMSCs, 2.5 x 10^4 cells) were pre-seeded on 0% and 1% RGO-CPCs disk (diameter of 6 mm), incubated for 4 hours, and then transplanted into the subcutaneous spaces of immunocompromised mice (NIH-bg-nu/nu-xid, Harlan Sprague Dawley, Indianapolis, IN, USA). Human ABMSCs which were inserted into polycaprolactone tube (diameter of 3 mm) were used as a negative control, and the cells mixed with Bio-Oss (Ed Geistlich Sons, Wolhusen, Switzerland) powder, a bovine bone derivative, as a positive control for transplantation. Samples (n = 5) were obtained after 12 weeks.

4.1.8.2. In vivo transplantation of RGO-CPCs at critical-size defects of rat calvaria

A second animal model using rat calvarial defects was designed to evaluate the effects of RGO-CPCs on regeneration capacities of bony structures without transplantation of cells. 0% and 0.01% RGO-CPCs were implanted into critical-size calvarial defects in twelve Sprague Dawley rats. 8-mm-diameter bony defects were made, and copious irrigation with sterile saline and hemostasis was performed. The critical-size defects in the control group received only a blood clot as a negative control, and Bio-Oss powder was used as a positive control. Sample harvesting was performed after 8 weeks.

4.1.8.3. Tissue preparation and histology

The transplanted hABMSCs samples and the calvarial segments were dissected carefully and samples were immersed in 4% paraformaldehyde then kept for an additional 24 hours. After being decalcified in a 10% EDTA (pH 7.4) solution, the specimens were embedded in paraffin. Serial 5-μm-thick sections were cut and stained with hematoxylin/eosin (H/E) for histological analysis. For

immunohistochemistry, transplanted hABMSCs samples were incubated overnight at 4℃ with rabbit polyclonal bone sialoprotein (BSP) (SC-59772, Santa Cruz Biotechnology) antibody at a dilution of 1:200. Sections were then incubated with secondary antibodies, anti-rabbit IgG, at room temperature for 30 min and reacted with the avidin–biotin-peroxidase complex (Vector Laboratory, Burlingame, CA). Signals were converted using a DAB kit (Vector Laboratory). Hematoxylin was used for staining of nuclei.

4.1.9. Electromagnetic stimulation

Electromagnetic stimulation was applied on RGO-CPCs. Their efficacy was evaluated via ARS. rASCs were fed with α-MEM and DMEM media to which 50 μg/mL ascorbate-2-phosphate (Sigma-Aldrich, WI, Milwaukee) and 10 μM dexamethasone (Sigma-Aldrich, WI, Milwaukee) were added for 2, 3, and 4 weeks, respectively. The PEMFs were irradiated using a solenoid. Electric signals, of which condition was square wave, ±5 V, 50 Hz-frequency, and 50%-duty cycle, were generated using a function generator. The condition of resultant PEMFs was 0.6 ± 0.05 mT with 50 Hz and expose time on samples was 30 min/day. Calcium precipitation of the ECM was visualized by staining

with ARS (Sigma-Aldrich, WI, Milwaukee). Briefly, the ethanol-fixed cells and matrix were stained for 1 hour with 40 mM ARS (pH 4.2) and extensively rinsed with water. After photography, the bound stain was eluted with 10% (wt/vol) cetylpyridinium chloride, and the ARS in samples was quantified by measuring the absorbance at 544 nm.

4.1.10. Statistical analysis

Statistical analyses were performed using the Statistical Analysis System (SAS) for Windows Ver. 9.4 (SAS Institute). The least significant difference (LSD) method and unpaired Student's t-tests were used to compare the means of the properties of the RGO-CPCs. The level of significance was $p < 0.05$.

4.2. Results

4.2.1. Characteristics of RGO-CPCs

To investigate the effects of RGO on the characteristics of CPCs, the morphological, chemical, and mechanical characteristics were evaluated to reveal the influence of RGO on natural CPCs. We first examined their morphology. As the inset of Fig. 4.1A indicated, bone cements became darker with increasing of RGO. According to the SEM results (Fig. 4.1A), their microstructural morphology became smoother as the RGO concentration increased. EDS evaluated the presence of graphene (Fig. 4.2). All samples showed carbon peak because CS, used as setting agent and having carbon in its back bone, was in all samples. Thus, by EDS we could not properly measure the presence of RGO. Instead, mapping analysis revealed that carbon atoms showed an even distribution, verifying that RGO was not aggregated and distributed well in the RGO-CPCs. Then, we examined the chemical properties of RGO-CPCs. In the XRD results, peaks were present at 25.4, 28.96, 31.38, 39.06, 45.76, and 48.6°, showing typical peaks of HA. (Fig. 4.1B) Further, at approximately 25° the peaks representing RGO were shown on 0.1% RGO and 1% RGO. In the Raman spectroscopy, all samples exhibited peaks at 270, 300 (2[(Ca_{II})3-(OH)] sublattice of hexagonal HA),

455 (ν_2 PO_4), 615 (ν_4 PO_4), 986 (ν_1 PO_4), and 1074 cm^{-1} (ν_3 PO_4), which are representative of HA bands. (Fig. 4.2C) Further, 0.1 and 1% RGO had 1398 (D) and 1696 (G) peaks, verifying the presence of RGO. Figures 4.1D and E show the XPS results of No and 1% RGO. In Fig. 4.1D, Ca2p3, P2p3, O1s, N1s, and C1s peaks were present. Fig. 4.1E shows the C1s peaks in detail. In these results, it was shown that the C-C peak of 1% RGO was drastically increased in comparison to No RGO.

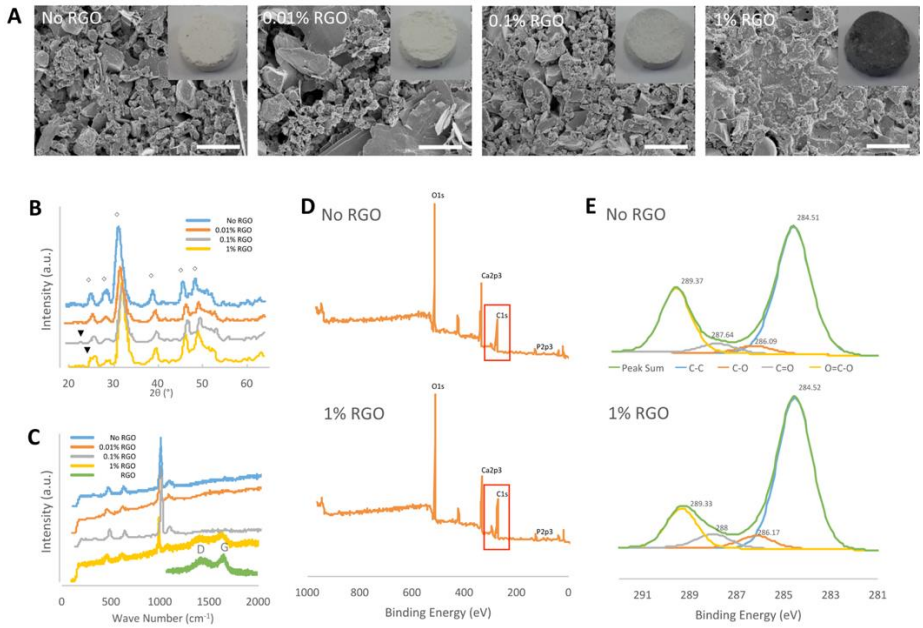

Fig. 4.1. Characteristics of RGO-CPCs (A) Morphological analysis. RGO-CPCs became darker as the RGO concentration increased. (inset) According to the FESEM results, the surface of RGO-CPCs aggregated more with the increased RGO concentration. Scale bars = 3 μm. (B) XRD results. HA specific peaks were present in all samples. In 0.1 and 1% RGO, new peak representing RGO was present at approximately 25°. (C) Raman spectroscopy results. Hydroxyapatite specific peaks were shown in all samples. The peaks representing RGO were clearly shown in 1% RGO. (D) Widescan results of XPS. O1s, Ca2p3, C1s, and P2p3 peaks were observed. (E) C1s peak of No and 1% RGO. Increased C-C and C-O bands was observed, and decreased C-O=O was observed.

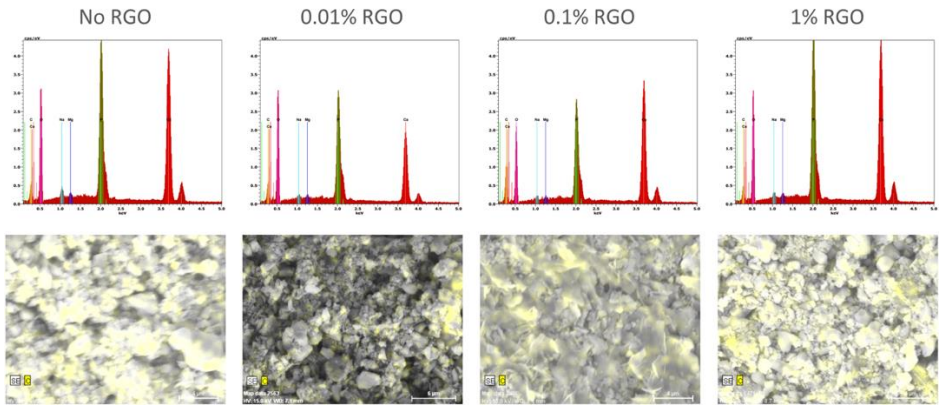

Fig. 4.2. EDS analysis results. By element mapping, an even distribution of RGO was confirmed.

We next examined mechanical properties of RGO-CPCs. (Fig. 4.3A) The elastic modulus of 0.1% and 1% RGO were significantly increased compared to No RGO. The maximum allowable strains of the RGO-CPCs were all increased, and the maximum compressive strength of 0.1 and 1% RGO were significantly increased compared with No RGO. To reveal the long-term behavior of RGO-CPCs in the human body, a soaking test was assessed, and their mass and mechanical properties were analyzed. (Fig. 4.3B) The mass of the RGO-CPCs was steadily decreased (not significantly), whereas the mechanical properties of the RGO-CPCs were gradually increased. In week 3, all of the mechanical properties of 0.1% RGO were excessively increased. In accordance with these results,

it was concluded that incorporation of RGO in CPCs highly strengthened the mechanical properties of RGO-CPCs.

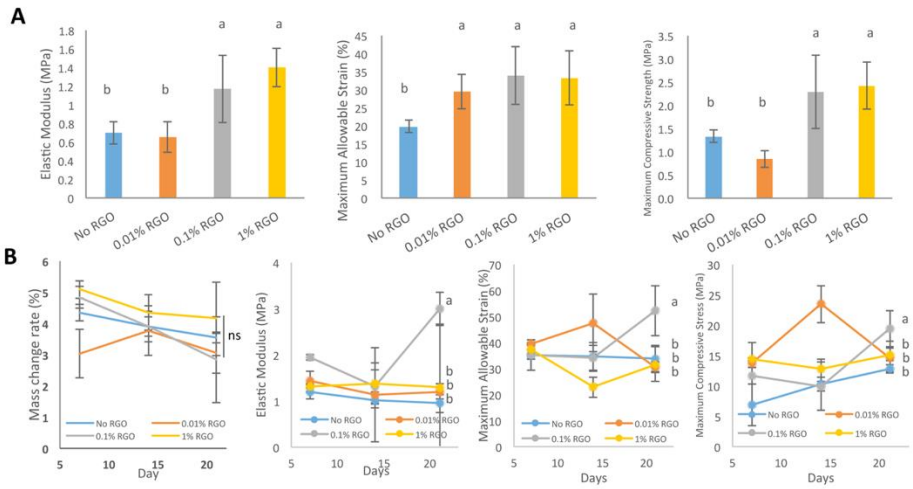

Fig. 4.3. Mechanical properties of RGO-CPCs. (A) Mechanical properties (elastic modulus, maximum allowable strain, and maximum compressive stress) of RGO-CPCs immediately after fabrication. Elastic modulus and maximum compressive stress of 0.1 and 1% RGO were significantly enhanced and the maximum allowable strain of all RGO-CPCs was increased compared to No RGO. (n = 10, LSD) (B) Soaking test results of RGO-CPCs. The mass change rate, elastic modulus, maximum allowable strain, and maximum compressive stress were investigated for 3 weeks. The elastic modulus, maximum allowable

strain, and maximum compressive stress of 0.1% RGO were significantly improved in comparison with the other samples. (n = 5, LSD)

4.2.2. *In vitro* study on MC3T3-E1

Next, an *in vitro* study was performed to evaluate whether RGO-CPCs are appropriate in clinical use for bone tissue engineering applications. We first used murine the osteoblast cell line - MC3T3-E1 - to determine the efficacy of RGO-CPCs on osteoblasts. First, in the cytotoxicity test, RGO-CPCs denoted slight toxicity at 12 hours. (Fig. 4.4A) However, their toxicity became marginal at 24 h. In the cell adhesion test, the cell adhesion rate was significantly decreased in 1% RGO. (Fig. 4.4B, inset) To determine the reason for decrease, ICC to stain the vinculin, the protein related with focal adhesion, was conducted. (Fig. 4.4C) On day 1, expression of vinculin decreased according to the increase of RGO. Nonetheless, the expression was increased in all RGO-CPCs on day 7, suggesting that the adverse effect of RGO on focal adhesion diminished with long-term cell adhesion. In the cell viability test, the optical density of the RGO-CPCs steadily decreased with the increase of RGO. (Fig. 4.4B)

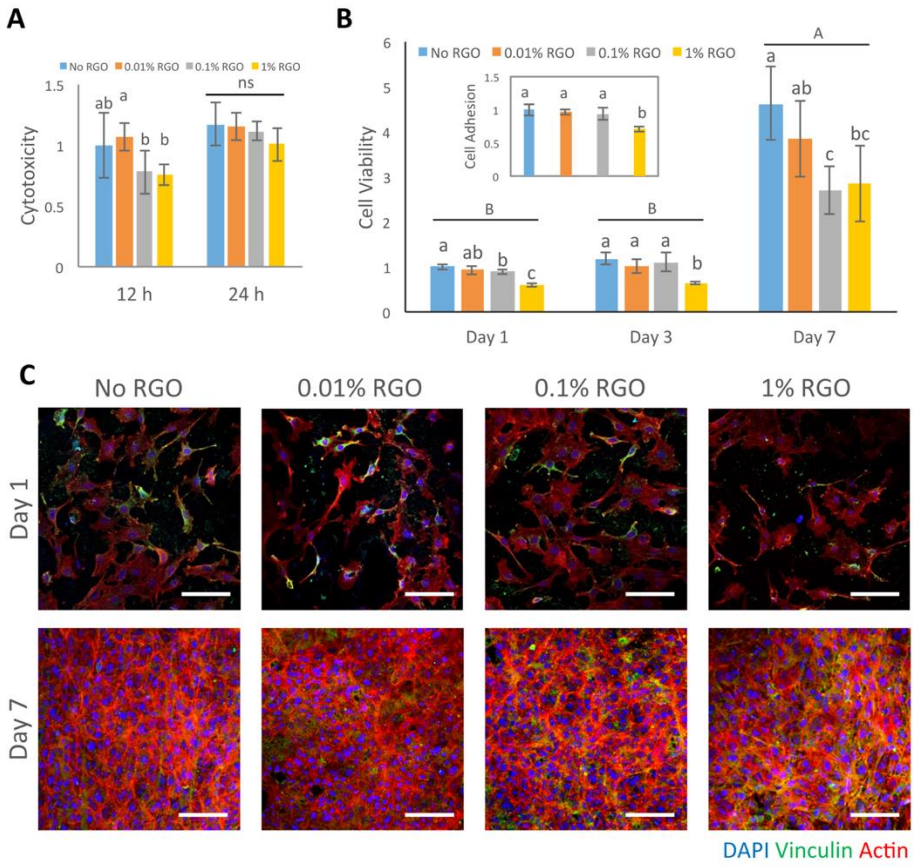

Fig. 4.4. *In vitro* study of MC3T3-E1. (A) Cytotoxicity result. The cytotoxicity of 0.01% RGO was the least at 12 hours, whereas the cytotoxicity of all CPCs was insignificant at 24 hours. (n = 5) (B) Cell viability result. On day 7, the cell viability of 0.1 and 1% RGO decreased significantly compared with No RGO. (n = 5, LSD) Inset: cell adhesion result. There is no significant difference except for 1% RGO. (n = 5, LSD) (C) ICC results. Vinculin expression decreased with increased of 1% RGO. Scale bars = 100 μm.

The cellular morphology of MC3T3-E1 on RGO-CPCs was also observed by FESEM. (Fig. 4.5) The cell density of RGO-CPCs decreased and their morphology became narrower as the RGO concentration increased.

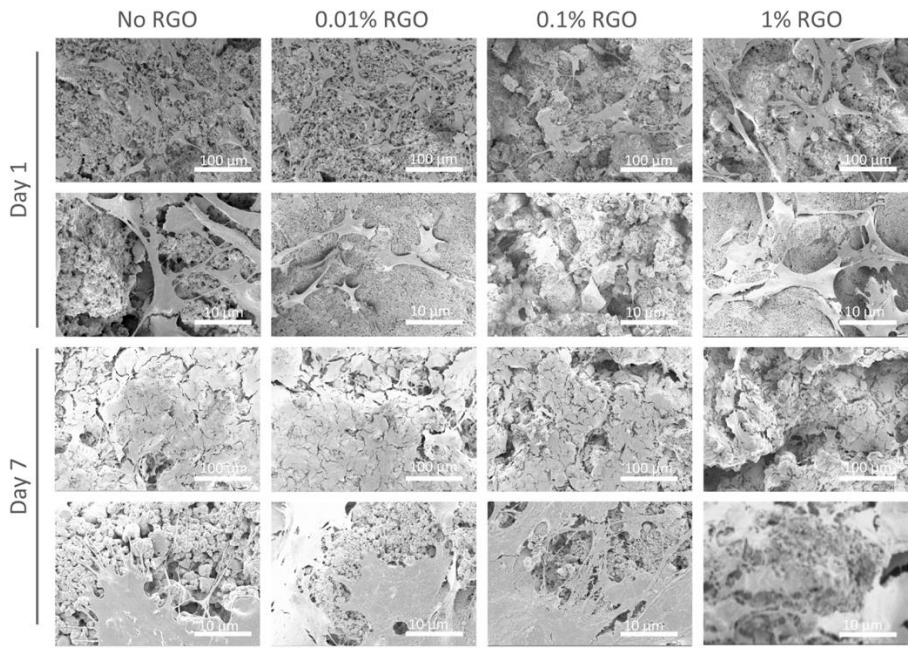

Fig. 4.5. Morphological analysis of MC3T3-E1 on RGO-CPCs. The growth was hampered and The shape became narrower with increased RGO concentration.

Additionally, a migration assay was conducted to determine if RGO-CPCs increase osteoconductivity. (Fig. 4.6) The 0.01% RGO showed the best wound closure on day 3.

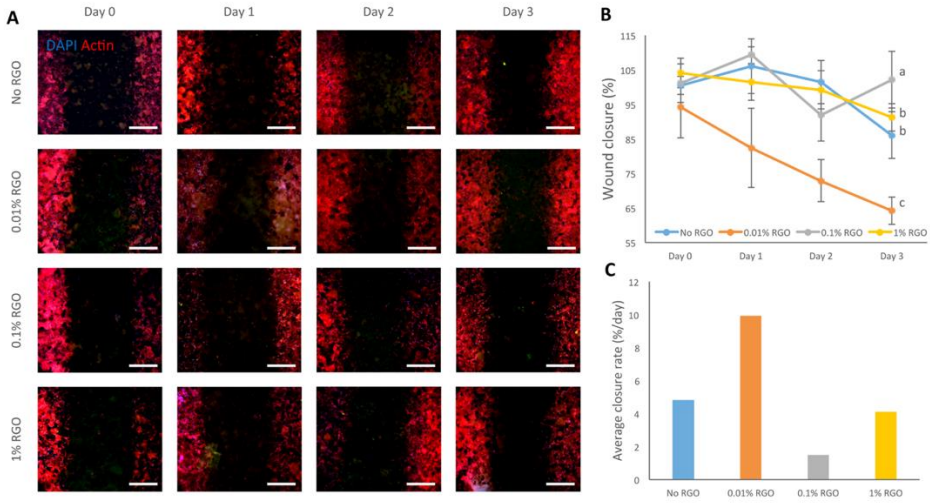

Fig. 4.6. Migration assay. (A) Representative pictures of the migration assay during 3 days. (B) Wound closure aspect during 3 days. (C) Average wound closure rate of RGO-CPCs. The 0.01% RGO marked fastest wound closure rate.

Next, we conducted an osteogenic differentiation study to examine the osteoinductivity of RGO-CPCs. First, protein expressions related with osteogenesis were checked by western blot. (Figs. 4.7A and B) Runx-2 and OCN were upregulated faster in 1% RGO, whereas ALP showed marginal results among all samples. In the ICC results, consistent with the western blot results, higher expression of OCN was observed on 1% RGO. (Fig. 4.7C) Furthermore, ARS was conducted to determine the calcium deposition. The highest calcium deposition rate was shown on 1% RGO. (Figs. 4.7D and E)

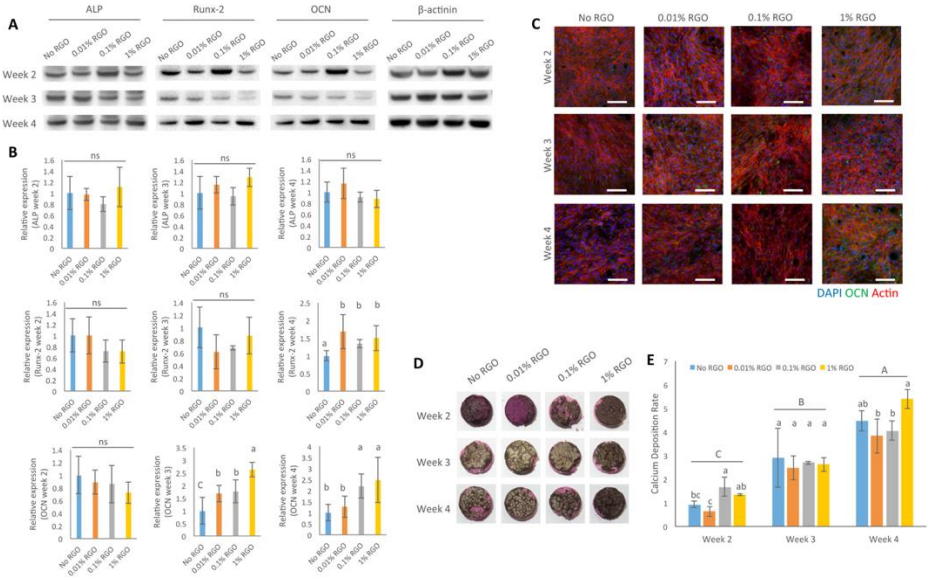

Fig. 4.7. Osteogenic differentiation study of MC3T3-E1 (A) Representative western blot result. ALP, Runx-2, OCN, and β-actinin expressions were evaluated during 4 weeks. (B) The relative expressions of osteogenic marker protein were calculated. The expression of ALP was not significantly different during 4 weeks. The expression of Runx-2 and OCN showed discrete differences in week 4. (C) ICC results. OCN expression for 4 weeks is depicted. At 4 weeks, 1% RGO had the highest OCN expression. Scale bars = 100 μm. (D) Representative images of ARS. (E) Quantitative analysis of ARS. The calcium deposition rate of 1% RGO in week 4 showed the highest value with significant difference. (n = 5, LSD)

4.2.3. *In vitro* study on rASCs

In addition to osteoblasts, stem cells also have a significant role in bone regeneration because the implantation of scaffolds with stem cells showed higher bone regeneration compared to scaffold implantation only. Hence, an *in vitro* study was performed on rASCs. The results were similar to those of MC3T3-E1. There was no difference between CPCs and RGO-CPCs at 12 h. In contrast, the cytotoxicity of RGO-CPCs was decreased at 24 hours (Fig. 4.8A). The cell adhesion rates of rASCs were not significant comparatively with No RGO, except for 1% RGO (Fig. 4.8B). ICC was investigated to evaluate the vinculin expression of rASCs on RGO-CPCs (Fig. 4.8D). Consistent with the cell adhesion rate, vinculin expression decreased with the increased graphene concentration. Cell viability was decreased with increased RGO (Fig. 4.8C).

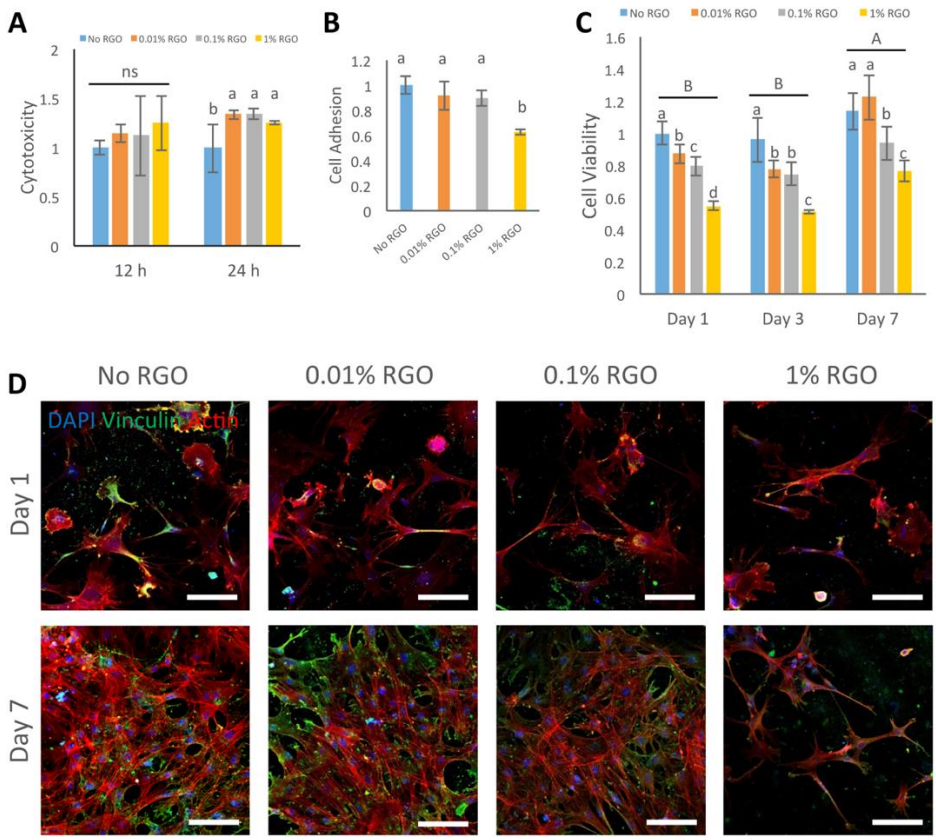

Fig. 4.8. *In vitro* study of rASCs. (A) Cytotoxicity result. The cytotoxicity of RGO-CPCs was lower than No RGO at 24 hours, whereas the cytotoxicity of all CPCs was insignificant at 12 hours. (n = 5) (B) Cell adhesion result. There is no significant difference except for 1% RGO. (n = 5, LSD) (C) Cell viability result. On day 7, the cell viability of 0.1 and 1% RGO significantly decreased compared with No RGO. (n = 5, LSD) (C) ICC result. Vinculin expression decreased with increased 1% RGO. Scale bars = 100 μm.

When the cellular morphology was observed by FESEM, the cell density and width decreased with increased RGO concentration (Fig. 4.9).

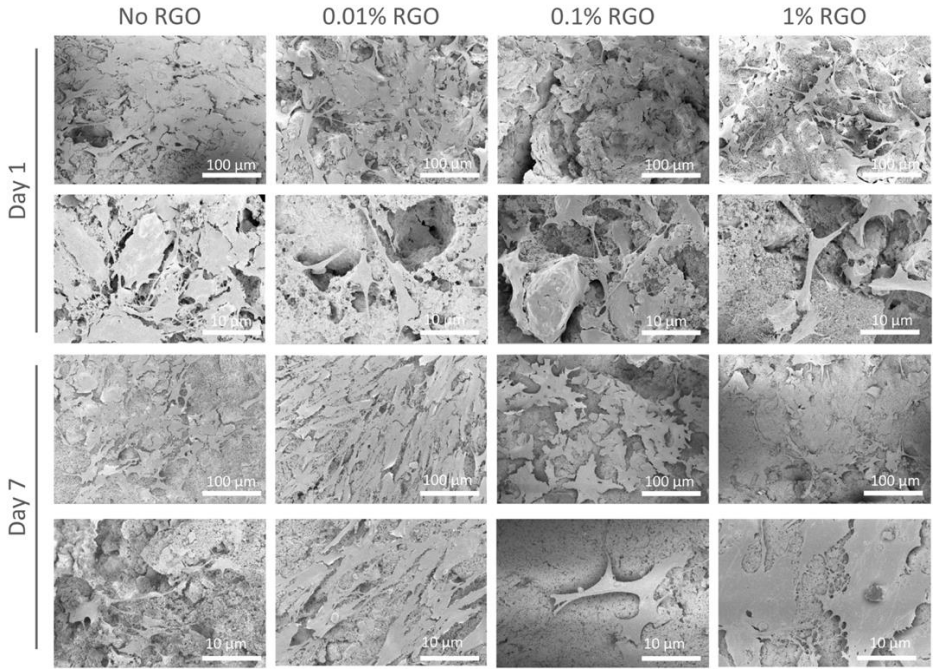

Fig. 4.9. Morphological analysis of rASCs on RGO-CPCs. The growth was hampered and the shape became narrower with increased RGO concentration.

When conducting the differentiation study, graphene bone cements accelerated osteogenic differentiation of rASCs (Fig. 4.10). In the western blotting and immunostaining results, the highest expression of OCN was recorded on 1% RGO (Figs. 4.10A, B, C, and D). Analogous results were observed in ARS assay (Figs. 4.10E and F). At 4 weeks, rASCs on 1% RGO showed the best calcium deposition.

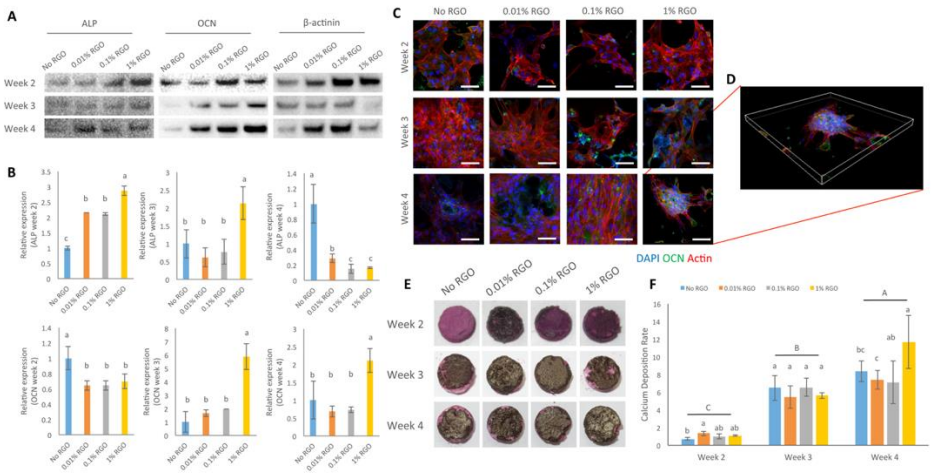

Fig. 4.10. Osteogenic differentiation study on rASCs (A) Representative western blot result. ALP, OCN expressions were evaluated during 4 weeks. (B) The relative expressions of osteogenic marker protein were calculated. In weeks 2 and 3, ALP expression was increasingly promoted

with increased RGO, indicating that the more RGO is incorporated, the faster the early stage of osteogenesis is. In weeks 3 and 4, OCN expression of 1% RGO was highly increased, indicating that 1% RGO underwent late stage osteogenesis earlier. (C) ICC result. OCN expression for 4 weeks is depicted. At 4 weeks, 1% RGO had the highest expression. Scale bars = 100 μm. (D) Three dimensional images of OCN expression on 1% RGO. Hemisphere-shaped cell aggregation indicates higher OCN expression. (E) Representative images of ARS. (F) Quantitative analysis of ARS. The calcium deposition rate of 1% RGO in week 4 had the highest value with a significant difference. (n = 5, LSD)

4.2.4. *In vivo* studies with or without hABMSCs

To evaluate whether RGO-CPCs could enhance bone regeneration without transplantation of any cells in vivo, 0% and 0.01% RGO-CPCs were implanted into critical sized defects of rat calvaria for twelve weeks (Fig. 4.11A). Bio-Oss was used as a positive control for bone regeneration. There was no evidence of inflammation in all groups. The calvarial defects in the control group showed formation of thin fibrous connective tissue layers and small amounts of bony growth at the margins of the defect, while the Bio-Oss group generated bone-like mineralized tissues on the border of Bio-Oss particles (Fig. 4.11B). In the 0.01% RGO group, more amounts of newly-formed bone tissues were regenerated in the periphery of surrounding the bony defects compared to the 0% RGO group. The regenerated mineralized tissues in the Bio-Oss and 1% RGO groups showed morphological characteristics of calvarial bone present at the margins of the defect, including typical osteocytes entrapped inside the matrix, and osteoblasts lining the outer margin of the mineralized tissue.

Based on the results from these in vitro experiments, hABMSCs-seeded-0% and 1% RGO-CPCs disc were transplanted into immunocompromised mice subcutaneously to evaluate the effects of both

RGO-CPCs on osteoblast differentiation of mesenchymal stem cells. Harvested samples were stained with H/E and immunostained with BSP antibody twelve weeks after transplantation. Histological analysis revealed that accumulation of extracellular matrices and collagen for generating mineralization foci were detected in the Bio-Oss and both RGO groups compared to the control group (Fig. 4.11C). 1% RGO group displayed osteoblast-like cells with abundant matrix formation. To confirm the osteoblast differentiation and mineralized matrix formation identified by morphology, we performed immunohistochemistry. BSP is regarded as specific markers of osteoblast differentiation. BSP expression was observed in the Bio-Oss group but weakly in the control group (Fig. 4.11D). In the 1% RGO group, the expression of BSP protein was detected in osteoblast-like cells that contact with the RGO-CPCs, however, there were few cells with BSP expression in the 0% RGO group.

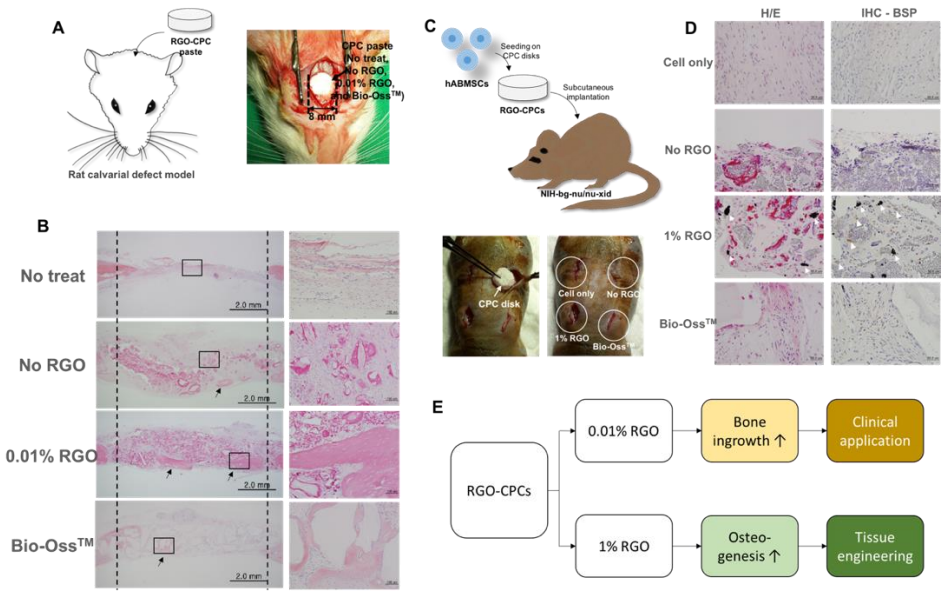

Fig. 4.11. *In vivo* study results. (A) No RGO, 0.01% RGO, and Bio-Oss™ were applied on rat calvarial defect models. (B) Twelve weeks later, 0.01% RGO successfully induced bone ingrowth. (C) The osteogenic capability of RGO-CPCs was assessed. HABMSCs were seeded onto the RGO-CPCs and those were subcutaneously implanted in nude mice. (D) Twelve weeks later, the hABMSCs on 1% RGO is similar with osteoblast-like cells while osteogenic differentiation deemed to be delayed in other groups. Moreover, 1% RGO strongly expressed BSP. (E) According to the *in vivo* results, 0.01% RGO successfully induced bone ingrowth. Hence, 0.01% RGO can be used directly in clinical application. 1% RGO accelerated the osteogenic differentiation of hABMSCs. The 1% RGO can be utilized in tissue engineering-based regeneration.

4.2.5. Electromagnetic stimulation upon RGO-CPCs

The efficacy of PEMFs on RGO-CPCs were investigated. The result was evaluated by ARS. On week 2, there's no significant difference among samples whereas 1% RGO under PEMFs exhibited significant difference on week 3.

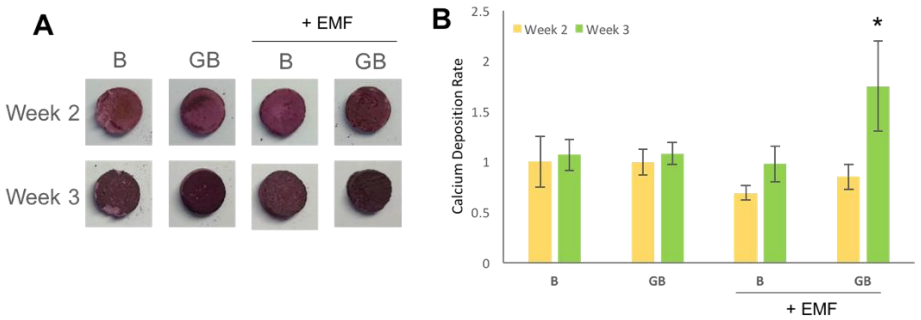

Fig. 4.12. ARS results of RGO-CPCs under PEMFs stimulation. (A) Representative results of ARS. (B) Quantitative results of ARS study. The PEMFs stimulation exhibited nonsignificant results on week 2 whilst the PEMFs stimulation induced significant result upon 1% RGO on week 3.

4.3. Discussion

CPCs have such good bioactivity that can be absorbed by surrounding tissue and be replaced with native tissues. However, the low mechanical strength of CPCs has remained a critical weakness. [18] There are few methods to reinforce the mechanical properties of natural CPCs because the existing methods work properly only in CaP synthesis. Likewise, not only osteoconductivity, but better osteoinductivity is important for natural CPCs. Thus, in this study, RGO was incorporated into the horse bone-derived natural CPCs to alleviate the disadvantages.

Horse bone powders, RGO, and CS solution were mixed thoroughly following the above mentioned concentration (Table 4.1) and were hardened in PDMS molds. As shown in Fig. 4.1A, RGO-CPCs became darker with the increase of the RGO concentration and their surface became more coagulated with the increase of the RGO concentration. The EDS results showed that RGO was evenly distributed although its precise location could not be proved. (Fig. 4.2) Next, the chemical characteristics of mixed powders were examined. In the XRD and Raman spectroscopy results, specific peaks of HA were observed. Specific peaks of RGO were also observed in RGO-CPCs. (Figs. 4.1B and C) From the results, it was confirmed that the main component of

sintered horse bone was HA, and RGO was incorporated in the powder mixture. In the XPS results, it was confirmed that C-C bonds are highly increased in 1% RGO, resulting in the presence of graphene. Next, the mechanical properties of the RGO-CPCs were measured. (Fig. 4.3) For the 0.1% and 1% RGO, the mechanical properties were enhanced almost twice by the insertion of RGO. Further, when the RGO-CPCs were soaked in SBF, 0.1% RGO showed outstanding improvement in mechanical properties. There were several reports that incorporation of or synthesis with GO enhanced the mechanical properties of HA and CS. The tensile strength and elastic modulus of GO/CS composite film were increased more than those of CS film. [41] The elastic modulus of GO/HA and the hardness of GO/HA/CS complex were evidently increased compared to HA. [96] Moreover, synthesis with HA and RGO improved the micro hardness, elastic modulus, and fracture toughness. [43] However, it has not been reported that the mixing and hardening of the HA/RGO/CS complex results in reinforcement of the mechanical properties of CPCs. Consequently, in our knowledge, this is the first report of the reinforcement of CPCs by the mixing of RGO/CS/HA composite. Together, this easy and simple method is highly suitable for

application in natural CPCs. Hence, this method is expected to enlarge the application range of natural CPCs.

After investigation of the morphological, chemical, and mechanical properties of RGO-CPCs, their *in vitro* behaviors were examined by MC3T3-E1 and rASCs. The adhesion rate of RGO-CPCs decreased as the RGO concentration increased. This was visually confirmed by vinculin ICC. As shown in Figs. 3.3C and 5D, vinculin expression decreased with the increase of the RGO concentration. Furthermore, the cell viability and migration study indicated that the results decreased with increasing of RGO concentration. There are two possible causes: (1) RGO-CPCs have cytotoxicity or (2) RGO-CPCs make cells promote other functionalities, such as osteogenic differentiation, rather than cell proliferation or migration. Considering their cytotoxicity result, the cytotoxicity of RGO-CPCs is insignificant (Figs. 4.4A and 8A). Moreover, the addition of the graphene family to HA for better osteogenesis has been recently reported. Tatavarty et al. reported that GO-CaP nanocomposite improved osteogenic differentiation of human mesenchymal stem cells (hMSCs) and [97] Li et al. reported that the chitosan–GO–HA composite enhanced osteogenesis of MG63. [96] Consequently, RGO-CPCs were anticipated to promote

osteogenesis of osteoblasts and rASCs. As expected, RGO-CPCs enhanced osteogenic differentiation of MC3T3-E1 and rASCs. The 1% RGO highly promoted osteogenic differentiation. In week 2, RGO most rapidly promoted early expression of ALP, the early marker of osteogenic differentiation (Figs. 4.7A and 10A). Subsequently, it promoted early expression of Runx-2 and OCN on week 3 and week 4, respectively. The results are consistent with the ICC and ARS results (Figs. 4.7C and 10C). The 1% RGO recorded the highest OCN expression and calcium deposition in week 4. Many researchers have been dedicated to advanced osteoinductiveness of CPCs. According to the researches, it was reported that the addition of Arg-Gly-Asp (RGD), fibronectin, and platelet concentration enhanced osteogenesis of human umbilical cord mesenchymal stem cells (hUCMSCs). [98] However, addition of carbon-based materials on CPCs related with osteoinductivity was not investigated. Thus, it was revealed that the utilization of carbon-based materials in natural CPCs will simultaneously enhance the mechanical properties and osteoinductivity. Thus, RGO-CPCs are anticipated to open the gate for the clinical application for natural CPCs. Based on the cell type, RGO-CPCs can be utilized differently. In the case of MC3T3-E1, 0.01% RGO showed the fastest migration result, whereas RGO-CPCs

represented comparatively low osteogenic capability. Hence, 0.01% RGO is suitable for bone wound healing. In contrast, 1% RGO demonstrated more effective osteogenic differentiation of rASCs than other RGO-CPCs. For bone regeneration, incorporation of 1% RGO and stem cells simultaneously would be more effective. Thus, when conducting *in vivo* study, 0.01% RGO were used in calvarial defect models and 1% RGO were used in stem cell differentiation. (Fig. 4.11) Consistent with *in vitro* study, 0.01% RGO promoted bone ingrowth. 1% RGO promoted osteogenic differentiation of hABMSCs. It is anticipated that 0.01% RGO is proper to be used in clinical applications. Further, 1% RGO is expected to be used in tissue engineering-based regeneration.

The use of pure RGO instead of GO or functionalized RGO is also notable. There were several reports on the use of GO in synthesis with HA for reinforcement of mechanical properties. [42, 99] Functionalized RGO [100] and RGO synthesized with HA [43] have been reported, as well. However, our research is, in our knowledge, the first report to use pure RGO in the study of CPCs. The use of pure RGO has several advantages: (1) Ease of fabrication. Simple mixing results in the easy fabrication process maintaining the reinforced mechanical properties. (2) Better promotion of osteogenesis. Lee et al. reported

osteogenic capability of graphene is better than GO. [37] Hence, RGO may promote better osteoinductivity than GO. (3) Good biodegradability. Although the biodegradability of RGO is worse than that of GO, it is degradable by enzymes. Hence, when conducting *in vivo* study, its toxicity is not a significant matter. (4) Utilization of the functionality of graphene. For example, exposure on graphene sheets could induce microelectric current. [101] If RGO is incorporated in CPCs, microelectric current, which can cause synergistic effects on osteogenic differentiation, would be induced by exposure in electromagnetic field. Consequently, it would result in synergic effects of graphene and microelectric current on bone regeneration. Furthermore, its unique properties, including high elastic modulus and thermal properties can be used in tissue regeneration. The incorporation of RGO on CPCs may provoke synergic effects in tissue engineering. As a preliminary study, their efficacy were investigated on No RGO and 1% RGO using ARS study. As a result, 1% RGO under PEMFs exhibited significant increase of calcium deposition on week 3. Although further study is required, it was established that collaboration of RGO-CPCs and PEMFs enhanced the osteogenic differentiation of rASCs. Consistent results will be

expected in *in vivo* study as well as clinical study. Consequently, RGO-CPCs and PEMFs will be a good method for bone regeneration.

5. Future Perspectives

5.1. Application of RGO

In this study, RGO, instead of GO or functionalized GO, were used. The use of pure RGO has several advantages: (1) Ease of fabrication. Simple mixing results in the easy fabrication process maintaining the reinforced mechanical properties. (2) Better promotion of osteogenesis. Lee et al. reported osteogenic capability of graphene is better than GO. Hence, RGO may promote better osteoinductivity than GO. (3) Good biodegradability. Although the biodegradability of RGO is worse than that of GO, it is degradable by enzymes. Hence, when conducting *in vivo* study, its toxicity is not a significant matter. (4) Utilization of the functionality of graphene. For example, exposure on graphene sheets could induce microelectric current. If RGO is incorporated in CPCs, microelectric current, which can cause synergistic effects on osteogenic differentiation, would be induced by exposure in electromagnetic field. It would result in synergic effects of graphene and microelectric current on bone regeneration. Furthermore, its unique properties, including high elastic modulus and thermal properties can be used in tissue regeneration. The incorporation of RGO on CPCs may

provoke synergic effects in tissue engineering. Consequently, it is expected that RGO would be utilized on traditional tissue engineered approach and derive optimistic results.

5.2. Induction of PEMFs on RGO-basted platforms

The system which induces PEMFs on RGO-based platform is anticipated to overcome the limitation of established RGO-based platforms for stem cell and tissue engineering. RGO is a kind of graphene family, made by reducing oxygen species on GO. Even though it is one of graphene subfamily, its purity cannot overcome the graphene fabricated by chemical vapor deposition (CVD) method. The electric resistance of RGO-adsorbed substrates is much higher than that of CVD graphene not only for its impurity but also the disconnection of RGO each other, resulting in disconnection resistance. Thus, these days the RGO-based systems are not preferred as platforms inducing mechanical stimulations in tissue engineering. By the way, invoking electric currents by PEMFs would resolve this problem. Because induced electric currents can be generated on local area, the substrate doesn't have to be connected each other, that is, this systems can overcome disconnection problem.

Another advantage of this system is that this system can be applied in the traditional tissue engineered scaffolds. By incorporating RGO, this system can be easily combined with them. It was known that RGO is hard to apply in tissue engineering because it is not well dispersed in organic or inorganic solvent. However, RGO can be dispersed well if the size of RGO is small enough. Moreover, it can be applicable in clinical study as well as *in vivo* study by combining with biodegradable scaffolds. Particularly, EMFs can be exerted on the transplanted scaffolds noninvasively. Thus, this system can be easily applied in clinical study as well as *in vivo* study. Owing to implanting stimulators in the wound area, other stimulation systems including electrical and light have limitations to be applied in *in vivo* study. On the other hand, EMFs stimulation is already commercialized in clinics for theraputic applications. Thus, EMFs stimulation system would come true in tissue engineering-based therapy. That would become a turning point in tissue engineering and regenerative medicine.

6. Conclusion

In this doctoral thesis, graphene-based nanostructural platforms were fabricated and their morphological, chemical, mechanical, and cellular features were investigated. Further, its electromagnetic properties were applied and assessed on stem cell and tissue engineering. First, RGO substrates and PEMFs were applied to hABMSCs and its efficacy to differentiation is evalutated. RGO+PEMFs enhanced cell viability. It also improved the expression of vinculin and fibronectin, related with focal adhesion and ECM. The RGO+PEMFs enhanced osteogenesis as well as neurogenesis and adipogenesis. Not only the PEMFs but also induced electric current synergically enhanced the multidifferentiation of hABMSCs. This system would become a turning point in tissue engineering and regenerative medicine. It can be applicable in clinical study as well as *in vivo* study by combining it with many biodegradable scaffolds. Particularly, because EMFs can be exerted on the transplanted scaffolds noninvasively, this system can be easily applied in clinical study as well as *in vivo* study. Thus, it is expected that EMFs stimulation system would come true in tissue engineering-based therapy. That would become a turning point in tissue engineering and regenerative medicine. Second, a new method to incorporate RGO into natural CPCs for

reinforcing the mechanical properties and osteoinductivity simultaneously is developed for bone tissue engineering. RGO-CPCs had enhanced mechanical properties, including elastic modulus, maximum allowable strain, and maximum compressive strength. In the soaking test, the mechanical properties of the RGO-CPCs were enhanced in comparison with CPCs. The RGO-CPCs not only had low cytotoxicity but also improved osteogenic differentiation of MC3T3-E1 and rASCs compared to CPCs. Furthermore, collaborative study of RGO-CPCs and PEMFs resulted in significant increase, consistent with former study. In conclusion, the RGO-CPCs are expected to overcome the flaws of formerly developed CPCs and open the gate for clinical application in bone repair and regeneration.

7. References

[1] Langer, R. and J.P. Vacanti. 1993. Tissue engineering. Science (New York, N.Y.) 260(5110):920-926.

[2] Seonwoo, H., S.W. Kim, J. Kim, T. Chunjie, K.T. Lim, Y.J. Kim, S. Pandey, P.H. Choung, Y.H. Choung and J.H. Chung. 2013. Regeneration of chronic tympanic membrane perforation using an EGF-releasing chitosan patch. Tissue engineering. Part A 19(17-18):2097-2107.

[3] Kim, J., S.W. Kim, S.J. Choi, K.T. Lim, J.B. Lee, H. Seonwoo, P.H. Choung, K. Park, C.S. Cho, Y.H. Choung and J.H. Chung. 2011. A healing method of tympanic membrane perforations using three-dimensional porous chitosan scaffolds. Tissue engineering. Part A 17(21-22):2763-2772.

[4] Zhang, J., W. Liu, V. Schnitzler, F. Tancret and J.M. Bouler. 2014. Calcium phosphate cements for bone substitution: Chemistry, handling and mechanical properties. Acta biomaterialia 10(3):1035-1049.

[5] Derby, B. 2012. Printing and prototyping of tissues and scaffolds. Science (New York, N.Y.) 338(6109):921-926.

[6] Dvir, T., B.P. Timko, D.S. Kohane and R. Langer. 2011. Nanotechnological strategies for engineering complex tissues. Nature nanotechnology 6(1):13-22.

[7] Kim, J., H.N. Kim, K.T. Lim, Y. Kim, H. Seonwoo, S.H. Park, H.J. Lim, D.H. Kim, K.Y. Suh, P.H. Choung, Y.H. Choung and J.H. Chung. 2013. Designing nanotopographical density of extracellular matrix for controlled morphology and function of human mesenchymal stem cells. Scientific reports 3:3552.

[8] Shao, S., S. Zhou, L. Li, J. Li, C. Luo, J. Wang, X. Li and J. Weng. 2011. Osteoblast function on electrically conductive electrospun PLA/MWCNTs nanofibers. Biomaterials 32(11):2821-2833.

[9] Galvan-Garcia, P., E.W. Keefer, F. Yang, M. Zhang, S. Fang, A.A. Zakhidov, R.H. Baughman and M.I. Romero. 2007. Robust cell migration and neuronal growth on pristine carbon nanotube sheets and yarns. Journal of biomaterials science. Polymer edition 18(10):1245-1261.

[10] Roldo, M. and D.G. Fatouros. 2013. Biomedical applications of carbon nanotubes. Annual Reports on the Progress of Chemistry - Section C 109:10-35.

[11] Goenka, S., V. Sant and S. Sant. 2014. Graphene-based nanomaterials for drug delivery and tissue engineering. Journal of controlled release : official journal of the Controlled Release Society 173:75-88.

[12] Kim, J., K.S. Choi, Y. Kim, K.T. Lim, H. Seonwoo, Y. Park, D.H. Kim, P.H. Choung, C.S. Cho, S.Y. Kim, Y.H. Choung and J.H. Chung. 2013. Bioactive effects of graphene oxide cell culture substratum on structure and function of human adipose-derived stem cells. Journal of biomedical materials research. Part A 101(12):3520-3530.

[13] Yang, X., Y. Tu, L. Li, S. Shang and X.M. Tao. 2010. Well-dispersed chitosan/graphene oxide nanocomposites. ACS applied materials & interfaces 2(6):1707-1713.

[14] Yazyev, O.V. and M. Katsnelson. 2008. Magnetic correlations at graphene edges: basis for novel spintronics devices. Physical review letters 100(4):047209.

[15] Feynman, R. P.; Leighton, R. B.; Sands, M., *The Feynman Lectures on Physics, Desktop Edition Volume I*. Basic Books: **2013**; Vol. 1.

[16] Saliev, T.; Mustapova, Z.; Kulsharova, G.; Bulanin, D.; Mikhalovsky, S., Therapeutic potential of electromagnetic fields for tissue engineering and wound healing. *Cell proliferation* **2014,** *47* (6), 485-493.

[17] Pesce, M.; Patruno, A.; Speranza, L.; Reale, M., Extremely low frequency electromagnetic field and wound healing: implication of cytokines as biological mediators. *European cytokine network* **2013,** *24* (1), 1-10.

[18] Lacy-Hulbert, A.; Metcalfe, J. C.; Hesketh, R., Biological responses to electromagnetic fields. *The FASEB Journal* **1998,** *12* (6), 395-420.

[19] Ross, C. L.; Siriwardane, M.; Almeida-Porada, G.; Porada, C. D.; Brink, P.; Christ, G. J.; Harrison, B. S., The effect of low-frequency electromagnetic field on human bone marrow stem/progenitor cell differentiation. *Stem Cell Research* **2015,** *15* (1), 96-108.

[20] Lim, K.; Hexiu, J.; Kim, J.; Seonwoo, H.; Cho, W. J.; Choung, P.-H.; Chung, J. H., Effects of electromagnetic fields on osteogenesis of human alveolar bone-derived mesenchymal stem cells. *BioMed research international* **2013,** *2013*.

[21] Cho, H.; Seo, Y. K.; Yoon, H. H.; Kim, S. C.; Kim, S. M.; Song, K. Y.; Park, J. K., Neural stimulation on human bone marrow- derived mesenchymal stem cells by extremely low frequency electromagnetic fields. *Biotechnology progress* **2012,** *28* (5), 1329-1335.

[22] Baek, S.; Quan, X.; Kim, S.; Lengner, C.; Park, J.-K.; Kim, J., Electromagnetic fields mediate efficient cell reprogramming into a pluripotent state. *ACS nano* **2014,** *8* (10), 10125-10138.

[23] Lawrence, W. T., Physiology of the acute wound. *Clinics in plastic surgery* **1998,** *25* (3), 321-340.

[24] Sunkari, V. G.; Aranovitch, B.; Portwood, N.; Nikoshkov, A., Effects of a low-intensity electromagnetic field on fibroblast migration and proliferation. *Electromagnetic biology and medicine* **2011,** *30* (2), 80-85.

[25] Costin, G.-E.; A Birlea, S.; A Norris, D., Trends in wound repair: cellular and molecular basis of regenerative therapy using electromagnetic fields. *Current molecular medicine* **2012,** *12* (1), 14-26.

[26] Pilla, A. A., Nonthermal electromagnetic fields: from first messenger to therapeutic applications. *Electromagnetic biology and medicine* **2013,** *32* (2), 123-136.

[27] Sheikh, A. Q.; Taghian, T.; Hemingway, B.; Cho, H.; Kogan, A. B.; Narmoneva, D. A., Regulation of endothelial MAPK/ERK signalling and capillary morphogenesis by low-amplitude electric field. *Journal of The Royal Society Interface* **2012**, rsif20120548.

[28] Feng, L.; Wu, L.; Qu, X., New horizons for diagnostics and therapeutic applications of graphene and graphene oxide. *Advanced Materials* **2013,** *25* (2), 168-186.

[29] Gao, W.; Alemany, L. B.; Ci, L.; Ajayan, P. M., New insights into the structure and reduction of graphite oxide. *Nature chemistry* **2009,** *1* (5), 403-408.

[30] Li, J.-L.; Kudin, K. N.; McAllister, M. J.; Prud'homme, R. K.; Aksay, I. A.; Car, R., Oxygen-driven unzipping of graphitic materials. *Physical review letters* **2006,** *96* (17), 176101.

[31] Nair, R.; Blake, P.; Grigorenko, A.; Novoselov, K.; Booth, T.; Stauber, T.; Peres, N.; Geim, A., Fine structure constant defines visual transparency of graphene. *Science* **2008,** *320* (5881), 1308-1308.

[32] Mahanta, N. K.; Abramson, A. R. In *Thermal conductivity of graphene and graphene oxide nanoplatelets*, Thermal and Thermomechanical Phenomena in Electronic Systems (ITherm), 2012 13th IEEE Intersociety Conference on, IEEE: 2012; pp 1-6.

[33] Mao, H. Y.; Laurent, S.; Chen, W.; Akhavan, O.; Imani, M.; Ashkarran, A. A.; Mahmoudi, M., Graphene: promises, facts, opportunities, and challenges in nanomedicine. *Chemical reviews* **2013,** *113* (5), 3407-3424.

[34] Goenka, S.; Sant, V.; Sant, S., Graphene-based nanomaterials for drug delivery and tissue engineering. *Journal of Controlled Release* **2014,** *173*, 75-88.

[35] Park, S. Y.; Park, J.; Sim, S. H.; Sung, M. G.; Kim, K. S.; Hong, B. H.; Hong, S., Enhanced differentiation of human neural stem cells into neurons on graphene. *Advanced Materials* **2011,** *23* (36), H263-H267.

[36] Kim, J.; Park, S.; Kim, Y. J.; Jeon, C. S.; Lim, K. T.; Seonwoo, H.; Cho, S.-P.; Chung, T. D.; Choung, P.-H.; Choung, Y.-H., Monolayer Graphene-Directed Growth and Neuronal Differentiation of Mesenchymal Stem Cells. *Journal of biomedical nanotechnology* **2015,** *11* (11), 2024-2033.

[37] Kim, J.; Kim, Y.-R.; Kim, Y.; Lim, K. T.; Seonwoo, H.; Park, S.; Cho, S.-P.; Hong, B. H.; Choung, P.-H.; Chung, T. D., Graphene-incorporated chitosan substrata for adhesion and differentiation of human mesenchymal stem cells. *Journal of Materials Chemistry B* **2013,** *1* (7), 933-938.

[38] Park, J.; Park, S.; Ryu, S.; Bhang, S. H.; Kim, J.; Yoon, J. K.; Park, Y. H.; Cho, S. P.; Lee, S.; Hong, B. H., Graphene–Regulated Cardiomyogenic Differentiation Process of Mesenchymal Stem Cells by Enhancing the Expression of Extracellular Matrix Proteins and Cell Signaling Molecules. *Advanced healthcare materials* **2014,** *3* (2), 176-181.

[39] Hsiao, Y. S.; Kuo, C. W.; Chen, P., Multifunctional Graphene–PEDOT Microelectrodes for On- Chip Manipulation of Human Mesenchymal Stem Cells. *Advanced Functional Materials* **2013,** *23* (37), 4649-4656.

[40] Akhavan, O.; Ghaderi, E., Differentiation of human neural stem cells into neural networks on graphene nanogrids. *Journal of Materials Chemistry B* **2013,** *1* (45), 6291-6301.

[41] Li, W.; Wang, J.; Ren, J.; Qu, X., 3D Graphene Oxide–Polymer Hydrogel: Near- Infrared Light- Triggered Active Scaffold for Reversible Cell Capture and On- Demand Release. *Advanced Materials* **2013,** *25* (46), 6737-6743.

[42] Yazyev, O. V.; Katsnelson, M., Magnetic correlations at graphene edges: basis for novel spintronics devices. *Physical Review Letters* **2008,** *100* (4), 047209.

[43] Magnan B, Bondi M, Maluta T, Samaila E, Schirru L, Dall'Oca C. Acrylic bone cement: current concept review. Musculoskelet Surg. 2013;97:93-100.

[44] Maurer P, Bekes K, Gernhardt CR, Schaller HG, Schubert J. Comparison of the bond strength of selected adhesive dental systems to cortical bone under in vitro conditions. Int J Oral Maxillofac Surg. 2004;33:377-81.

[45] Brochu AB, Evans GA, Reichert WM. Mechanical and cytotoxicity testing of acrylic bone cement embedded with microencapsulated 2-octyl cyanoacrylate. J Biomed Mater Res B Appl Biomater. 2014;102:181-9.

[46] Zhang J, Liu W, Schnitzler V, Tancret F, Bouler JM. Calcium phosphate cements for bone substitution: chemistry, handling and mechanical properties. Acta Biomater. 2014;10:1035-49.

[47] Chow LC, Markovic M, Takagi S. A dual constant-composition titration system as an in vitro resorption model for comparing dissolution rates of calcium phosphate biomaterials. J Biomed Mater Res B Appl Biomater. 2003;65:245-51.

[48] Sobczak A, Kowalski Z, Wzorek Z. Preparation of hydroxyapatite from animal bones. Acta Bioeng Biomech. 2009;11:23-8.

[49] Lim KT, Kim JW, Kim J, Chung JH. Development and Evaluation of Natural Hydroxyapatite Ceramics Produced by the Heat Treatment of Pig Bones. J of Biosystems Eng. 2014;39:227-34.

[50] Barakat NA, Khalil K, Sheikh FA, Omran A, Gaihre B, Khil SM, et al. Physiochemical characterizations of hydroxyapatite extracted from bovine bones by three different methods: Extraction of biologically desirable HAp. Mater Sci Eng C. 2008;28:1381-7.

[51] Kim H, Rey C, Glimcher MJ. X-ray diffraction, electron microscopy, and Fourier transform infrared spectroscopy of apatite crystals isolated from chicken and bovine calcified cartilage. Calcif Tissue Int. 1996;59:58-63.

[52] Jang K-J, Cho WJ, Seonwoo H, Kim J, Lim KT, Chung P-H, et al. Development and Characterization of Horse Bone-derived Natural Calcium Phosphate Powders. J of Biosystems Eng. 2014;39:122-33.

[53] Zhang JT, Tancret F, Bouler JM. Fabrication and mechanical properties of calcium phosphate cements (CPC) for bone substitution. Mater Sci Eng C. 2011;31:740-7.

[54] Liu C, Shao H, Chen F, Zheng H. Effects of the granularity of raw materials on the hydration and hardening process of calcium phosphate cement. Biomaterials. 2003;24:4103-13.

[55] Gbureck U, Barralet JE, Spatz K, Grover LM, Thull R. Ionic modification of calcium phosphate cement viscosity. Part I: hypodermic injection and strength improvement of apatite cement. Biomaterials. 2004;25:2187-95.

[56] Lim KT, Baik SJ, Kim SW, Kim J, Seonwoo H, Kim J-W, et al. Development and characterization of fast-hardening composite cements composed of natural ceramics originated from horse bones and chitosan solution. Tissue Eng Regen Med. 2014;11:362-71.

[57] Sarda S, Fernandez E, Nilsson M, Balcells M, Planell JA. Kinetic study of citric acid influence on calcium phosphate bone cements as water-reducing agent. J Biomed Mater Res. 2002;61:653-9.

[58] Liu W, Zhang J, Weiss P, Tancret F, Bouler JM. The influence of different cellulose ethers on both the handling and mechanical properties of calcium phosphate cements for bone substitution. Acta Biomater. 2013;9:5740-50.

[59] Launey ME, Ritchie RO. On the fracture toughness of advanced materials. Adv Mater. 2009;21:2103-10.

[60] Novoselov KS, Geim AK, Morozov S, Jiang D, Zhang Y, Dubonos S, et al. Electric field effect in atomically thin carbon films. science. 2004;306:666-9.

[61] Kim KS, Zhao Y, Jang H, Lee SY, Kim JM, Kim KS, et al. Large-scale pattern growth of graphene films for stretchable transparent electrodes. Nature. 2009;457:706-10.

[62] Akhavan O, Ghaderi E, Emamy H, Akhavan F. Genotoxicity of graphene nanoribbons in human mesenchymal stem cells. Carbon. 2013;54:419-31.

[63] Kim J, Choi KS, Kim Y, Lim KT, Seonwoo H, Park Y, et al. Bioactive effects of graphene oxide cell culture substratum on structure and function of human adipose-derived stem cells. J Biomed Mater Res A. 2013;101:3520-30.

[64] Kim J, Kim Y-R, Kim Y, Lim KT, Seonwoo H, Park S, et al. Graphene-incorporated chitosan substrata for adhesion and differentiation of human mesenchymal stem cells. J Mater Chem B. 2013;1:933-8.

[65] Lee WC, Lim CHYX, Shi H, Tang LAL, Wang Y, Lim CT, et al. Origin of Enhanced Stem Cell Growth and Differentiation on Graphene and Graphene Oxide. ACS Nano. 2011;5:7334-41.

[66] Kim J, Park S, Kim YJ, Jeon CS, Lim KT, Seonwoo H, et al. Monolayer Graphene-Directed Growth and Neuronal Differentiation of Mesenchymal Stem Cells. J Biomed Nanotech. in press.

[67] Park SY, Park J, Sim SH, Sung MG, Kim KS, Hong BH, et al. Enhanced differentiation of human neural stem cells into neurons on graphene. Adv Mater. 2011;23:H263-H7.

[68] Tatavarty R, Ding H, Lu G, Taylor RJ, Bi X. Synergistic acceleration in the osteogenesis of human mesenchymal stem cells by graphene oxide-calcium phosphate nanocomposites. Chem Comm. 2014;50:8484-7.

[69] Yang X, Tu Y, Li L, Shang S, Tao X-m. Well-dispersed chitosan/graphene oxide nanocomposites. ACS appl Mater Interfaces. 2010;2:1707-13.

[70] Fan Z, Wang J, Wang Z, Ran H, Li Y, Niu L, et al. One-pot synthesis of graphene/hydroxyapatite nanorod composite for tissue engineering. Carbon. 2014;66:407-16.

[71] Baradaran S, Moghaddam E, Basirun W, Mehrali M, Sookhakian M, Hamdi M, et al. Mechanical properties and biomedical applications of a nanotube hydroxyapatite-reduced graphene oxide composite. Carbon. 2014;69:32-45.

[72] McMurray, R.J., N. Gadegaard, P.M. Tsimbouri, K.V. Burgess, L.E. McNamara, R. Tare, K. Murawski, E. Kingham, R.O. Oreffo and M.J. Dalby. 2011. Nanoscale surfaces for the long-term maintenance of mesenchymal stem cell phenotype and multipotency. Nature materials 10(8):637-644.

[73] Lutolf et al., Artificial stem cell niches. Adv. Mater (2013).

[74] Guilak et al., Control of stem cell fate by physical interactions with the extracellular matrix. Cell Stem Cell (2009).

[75] Vazin et al., Engineering strategies to emulate the stem cell niche. Trends in biotechnology (2010).

[76] Kim et al., Matrix nanotopography as a regulator of cell function. J. Cell Biol (2012).

[77] Place et al., Complexity in biomaterials for tissue engineering. Nat. Mater (2009).

[78] Lutolf et al., Designing materials to direct stem-cell fate. Nature (2009).

[79] Kim et al., Biomimetic Nanopatterns as Enabling Tools for Analysis and Control of Live Cells. Adv. Mater (2010).

[80] Ferreira et al., New opportunities: The use of nanotechnologies to manipulate and track stem cells. Cell Stem Cell (2008)

[81] Ku et al., Carbon-Based Nanomaterials for Tissue Engineering. Advanced healthcare materials (2012).

[82] Stout et al., Carbon nanotubes for stem cell control. Materials Today (2012).

[83] Baik et al., Carbon Nanotube Monolayer Cues for Osteogenesis of Mesenchymal Stem Cells. Small (2011).

[84] Chung et al., Biomedical Applications of Graphene and Graphene Oxide. Acc. Chem. Res (2013).

[85] Zhu et al., Graphene and Graphene Oxide: Synthesis, Properties, and Applications. Adv. Mater (2010).

[86] Allen et al., Honeycomb Carbon: A Review of Graphene. Chemical reviews (2010)

[87] Ozyilmaz et al., Graphene for Controlled and Accelerated Osteogenic Differentiation of Human Mesenchymal Stem Cells. ACS NANO (2011).

[88] Kim et al., Bioactive effects of graphene oxide cell culture substratum on structure and function of human adipose-derived stem cells. J Biomed Mater Res Part A (2013).

[89] Li et al., Three-dimensional graphene foam as a biocompatible and conductive scaffold for neural stem cells. SCIENTIFIC REPORTS (2013).

[90] Kim et al., Graphene-incorporated chitosan substrata for adhesion and differentiation of human mesenchymal stem cells. J. Mater. Chem. B (2013).

[91] Lee et al., Origin of Enhanced Stem Cell Growth and Differentiation on Graphene and Graphene Oxide. ACS NANO (2011).

[92] Chen et al., A graphene-based platform for induced pluripotent stem cells culture and differentiation. Biomaterials (2012).

[93] Kalbacova et al., Graphene substrates promote adherence of human osteoblasts and mesenchymal stromal cells. Carbon (2010).

[94] Park et al., Enhanced Differentiation of Human Neural Stem Cells into Neurons on Graphene. Adv. Mater (2011).

[95] Wang et al., Fluorinated Graphene for Promoting Neuro-Induction of Stem Cells. Adv. Mater (2012).

[96] Li M, Wang Y, Liu Q, Li Q, Cheng Y, Zheng Y, et al. In situ synthesis and biocompatibility of nano hydroxyapatite on pristine and chitosan functionalized graphene oxide. J Mater Chem B. 2013;1:475-84.

[97] Tatavarty R, Ding H, Lu G, Taylor RJ, Bi X. Synergistic acceleration in the osteogenesis of human mesenchymal stem cells by graphene oxide–calcium phosphate nanocomposites. Chem Comm. 2014.

[98] Thein-Han W, Liu J, Xu HH. Calcium phosphate cement with biofunctional agents and stem cell seeding for dental and craniofacial bone repair. Dent Mater. 2012;28:1059-70.

[99] Gonçalves G, Cruz SM, Ramalho A, Grácio J, Marques PA. Graphene oxide versus functionalized carbon nanotubes as a reinforcing agent in a PMMA/HA bone cement. Nanoscale. 2012;4:2937-45.

[100] Zanin H, Saito E, Marciano FR, Ceragioli HJ, Granato AEC, Porcionatto M, et al. Fast preparation of nano-hydroxyapatite/superhydrophilic reduced graphene oxide composites for bioactive applications. J Mater Chem B. 2013;1:4947-55.

[101] Yazyev OV, Katsnelson M. Magnetic correlations at graphene edges: basis for novel spintronics devices. Phys Rev Lett. 2008;100:047209.

[102] García-Gareta, E.; Coathup, M. J.; Blunn, G. W., Osteoinduction of bone grafting materials for bone repair and regeneration. *Bone* **2015,** *81*, 112-121.

[103] Ellis, K. M.; O'Carroll, D. C.; Lewis, M. D.; Rychkov, G. Y.; Koblar, S. A., Neurogenic potential of dental pulp stem cells isolated from murine incisors. *Stem cell research & therapy* **2014,** *5* (1), 30.

[104] Foley, B.; Clewell, R.; Deisenroth, C., Development of a Human Adipose-Derived Stem Cell Model for Characterization of Chemical Modulation of Adipogenesis. *Applied In Vitro Toxicology* **2015,** *1* (1), 66-78.

[105] Yi, C.; Liu, D.; Fong, C.-C.; Zhang, J.; Yang, M., Gold nanoparticles promote osteogenic differentiation of mesenchymal stem cells through p38 MAPK pathway. *Acs Nano* **2010,** *4* (11), 6439-6448.

[106] Zhang, R.; Lee, P.; Lui, V. C.; Chen, Y.; Liu, X.; Lok, C. N.; To, M.; Yeung, K. W.; Wong, K. K., Silver nanoparticles promote osteogenesis of mesenchymal stem cells and improve bone fracture healing in

osteogenesis mechanism mouse model. *Nanomedicine: Nanotechnology, Biology and Medicine* **2015,** *11* (8), 1949-1959.

[107] Baik, K. Y.; Park, S. Y.; Heo, K.; Lee, K. B.; Hong, S., Carbon nanotube monolayer cues for osteogenesis of mesenchymal stem cells. *small* **2011,** *7* (6), 741-745.

[108] Lee, W. C.; Lim, C. H. Y.; Shi, H.; Tang, L. A.; Wang, Y.; Lim, C. T.; Loh, K. P., Origin of enhanced stem cell growth and differentiation on graphene and graphene oxide. *ACS nano* **2011,** *5* (9), 7334-7341.

[109] (a) Seonwoo, H.; Kim, S. W.; Kim, J.; Chunjie, T.; Lim, K. T.; Kim, Y. J.; Pandey, S.; Choung, P.-H.; Choung, Y.-H.; Chung, J. H., Regeneration of chronic tympanic membrane perforation using an EGF-releasing chitosan patch. *Tissue Engineering Part A* **2013,** *19* (17-18), 2097-2107; (b) Zagris, N., Extracellular matrix in development of the early embryo. *Micron* **2001,** *32* (4), 427-438.

[110] McMurray, R. J.; Gadegaard, N.; Tsimbouri, P. M.; Burgess, K. V.; McNamara, L. E.; Tare, R.; Murawski, K.; Kingham, E.; Oreffo, R. O.; Dalby, M. J., Nanoscale surfaces for the long-term maintenance of mesenchymal stem cell phenotype and multipotency. *Nature materials* **2011,** *10* (8), 637-644.

[110] Balint, R.; Cassidy, N. J.; Cartmell, S. H., Electrical stimulation: a novel tool for tissue engineering. *Tissue Engineering Part B: Reviews* **2012,** *19* (1), 48-57.